Graduate School ETD Form 9
(Revised 12/07)

PURDUE UNIVERSITY
GRADUATE SCHOOL
Thesis/Dissertation Acceptance

This is to certify that the thesis/dissertation prepared

By Rui Wu

Entitled

Comb-based Radio Frequency Photonic Filtering: Principles, Applications and Opportunities

For the degree of Doctor of Philosophy

Is approved by the final examining committee:

ANDREW M. WEINER
Chair

ALEXANDRA BOLTASSEVA

DAVID D. NOLTE

DIMITRIOS PEROULIS

To the best of my knowledge and as understood by the student in the *Research Integrity and Copyright Disclaimer (Graduate School Form 20)*, this thesis/dissertation adheres to the provisions of Purdue University's "Policy on Integrity in Research" and the use of copyrighted material.

Approved by Major Professor(s): ANDREW M. WEINER

Approved by: V. Balakrishnan 04-22-2013
Head of the Graduate Program Date

COMB-BASED RADIO FREQUENCY PHOTONIC FILTERING: PRINCIPLES, APPLICATIONS AND OPPORTUNITIES

A Dissertation

Submitted to the Faculty

of

Purdue University

by

Rui Wu

In Partial Fulfillment of the

Requirements for the Degree

of

Doctor of Philosophy

May 2013

Purdue University

West Lafayette, Indiana

This dissertation is dedicated to my parents Baoguang Wu and Junhong Xie, from whom I knew the power of dream and persistence.

ACKNOWLEDGMENTS

I would like to thank my advisor Prof. Andrew M. Weiner for his great guidance throughout my graduate studies, from whom I learnt very much about optics. More importantly, Prof. Weiner and Mrs. Brenda Weiner set me two role models what a decent person should be like. I am very grateful to Prof. Weiner for giving me this valuable opportunity to pursue my academic dream under his direction. I would also like to thank Prof. Dimitrios Peroulis, Prof. David Nolte, and Prof. Alexandra Boltasseva for serving in my advisory committee and for their helpful comments.

My thanks go to our lab manager Dr. Daniel E. Leaird for his invaluable technical support. I appreciate the administrative assistances from Ms. Dee Dee Dexter through all my years at Purdue. I would also like to thank my current and former colleagues Dr. Christopher M. Long, Dr. Victor Torres-Company, Dr. V.R. Supradeepa, Prof. Dongsun Seo, Dr. Ehsan Hamidi, Dr. Fahmida Ferdous, Dr. Min Hyup Song, Dr. Li Xu, Dr. Hao Shen, Jian Wang, and many others for many research discussions and fruitful collaborations. I thank Prof. Xiaoguang Leo Liu from University of California, Davis for his introductory guidance to RF filters work.

In particular, I would like to thank Prof. Holly Wang, Kirk Cerny, Mary Dennis, Dr. Hongzi Liang, Jing Chen, Fengyuan Li, Dr. Zheng Zhang, Hailiang Chen, Dr. Feng Sheng and many other colleagues and friends for their assistance and supports during my service as the head of alumni communication committee and later president of Association of Purdue Chinese Alumni (APCA), through which I had an opportunity to serve our Purdue Chinese alumni community.

I am very grateful to Dr. Ezra Ip, my mentor at NEC Laboratories (Princeton, NJ) for the internship opportunity and his research guidance. I am also very thankful for the

great supports from Dr. Philip Ji, Dr. Ting Wang and many other colleagues at NEC laboratories.

I owe my great gratitude to the Kortebein's: Bill, Carol, Daniel, Laura (Mia), Kelsi, and Matthew, whom I regard as my American family. It is my great pleasure knowing them and being involved in many their family events. I was so grateful having Bill and Carol in my wedding in Montgomery, Alabama.

I am very thankful to have Uncle Kok-Wai (Bill) Chang & Auntie Maria Chang, Shandora Hassan (Mengxi Xiao) & Prof. Ray Hassan, Prof. Jun Chen & Xiaojin Liu, Auntie Susie Cheng & Prof. Heng-Wei Cheng, Prof. Ping Liu, Liya Men & Anna Haisi Yu, Lili Liu, and many others who are always very supportive and willing to lend an ear to me whenever I would like to share what happens in my life.

I am very grateful to Uncle Dr. Kok-Wai (Bill) Chang, Dr. Ingrid S. Lin, Dr. Kai Zhu, Dr. Raymond Chu, Prof. Jan Allebach, and Dr. Tingye Li for the invaluable discussions, encouragements and suggestions on my career. Unfortunately, Dr. Tingye Li passed away on December 27, 2012. He was a very kind and respected man.

I would like to dedicate this dissertation to the memory of my grandfather Deshan Wu. My grandpa Deshan Wu always encouraged me to study hard at school. He passed away in 2000 and cannot witness my getting PhD degree, one of the most glorious moments in my life.

I would like to thank my parents Baoguang Wu & Junhong Xie, my parents-in-law Albert & Hongbing Woolbright, my grandparents Zhenyi Xie & Hui Xu and all my other family members for their supports and love. I am trying my best to worth their blind proud of me. Particularly I would like to thank my beloved grandpa Zhenyi Xie, who has been a major source to motivate me to work hard and pursue my dreams. My grandpa is now suffering from both cancer and stroke. I hope he will recover soon.

Lastly, I would like to thank my beautiful wife Xuemin (Jenny) Ji, for her love and supports, and for making our legendary love story happen.

TABLE OF CONTENTS

Page

LIST OF FIGURES

Figure Page

Figure Page

Figure Page

Figure Page

Figure Page

LIST OF ABBREVIATIONS

CW	Continuous wave
DCF	Dispersion compensating fiber
EDFA	Erbium doped fiber amplifier
FSR	Free spectral range
FWHM	Full width at half maximum
FWM	Four wave mixing
HNLF	Highly nonlinear fiber
IM	Intensity modulator
MSSR	Mainlobe-to-sidelobe suppression ratio
MZM	Mach-Zehnder modulator
OSA	Optical spectrum analyzer
PC	Polarization controller
PM	Phase modulator
PS	Phase shifter
RF	Radio frequency
SMF	Single mode fiber
SNR	Signal to noise ratio
VNA	Vector network analyzer

ABSTRACT

Wu, Rui. Ph.D. Purdue University, May 2013. Comb-based radio frequency photonic filtering: principles, applications and opportunities. Major Professor: Andrew M. Weiner.

Photonic technologies have received tremendous attention for enhancement of radio-frequency (RF) systems, including control of phased arrays, analog-to-digital conversion, high-frequency analog signal transmission, and RF signal processing. Among the various applications, implementation of tunable electrical filters over broad RF bandwidths has been much discussed. However, realization of programmable filters with highly selective filter lineshapes, fast RF bandwidth reconfiguration and rapid passband frequency tunability has faced significant challenges. Phase modulated continuous-wave laser frequency combs have seen wide use in various applications such as wavelength division multiplexing networks, optical arbitrary waveform generation, and agile arbitrary millimeter wave generation. Using an optical frequency comb as a multiple carrier optical source offers new potential for achieving complex and tunable RF photonic filters. In this dissertation, I discuss about the generation and application of high-repetition-rate (10 GHz) electro-optic modulated optical frequency combs for our breakthroughs in implementing programmable RF photonic filters with highly selective filter lineshapes (>60 dB mainlobe-to-sidelobe suppression ratio), fast RF bandwidth reconfiguration (~20 ns reconfiguration speed) and rapid RF passband frequency tunability (~40 ns tuning speed).

1. INTRODUCTION

Radio-frequency (RF) photonics technology, in which RF signals are processed by means of photonics have drawn dramatic interests for enhancement of RF systems, including control of phased arrays, analog-to-digital conversion, high-frequency analog signal transmission, and RF signal processing. Among the various applications, implementation of high quality RF tunable filters over broad bandwidth is of great interest. However, realization of programmable RF filters with high selectivity, fast bandwidth reconfiguration, and rapid passband frequency tenability has faced significant challenges. Optical frequency comb, a multi-wavelength laser source provides very high degree of generation flexibility and overall comb shape reconfigurability, which offers new potential for achieving complex and tunable RF photonic filters. In this dissertation, I will present our approach to generate 10 GHz very high quality flat-topped and Gaussian shaped optical frequency comb based on electro-optic modulation schemes and nonlinear broadening technique. Based on the intentionally shaped optical frequency comb, we demonstrate our recent advancement in RF photonic filters with very rare high selectivity, fast bandwidth reconfiguration and rapid passband frequency tuning speed.

1.1. Optical frequency comb

In 2005, half Nobel physics prize was awarded to John Hall (University of Colorado at Boulder) and Theodor Hansch (Max Plank Institute) who are pioneering in optical frequency comb, a set of evenly spaced series of discrete spectral lines in frequency domain [1].

Figure 1.1(b) is a cartoon example of optical frequency comb and Figure 1.1(a) is its counterpart in time domain. Two attributes of a comb are (i) repetition frequency μ_r and

*Some of this chapter has been published in [41].

(ii) carrier offset frequency μ_0 . Any frequency can be denoted as the following expression:

$$\mu = \mu_0 + m\mu_r \tag{1.1}$$

where m is the order of comb line.

Two major approaches are heavily studied to generate optical frequency combs for different applications. One kind of comb is generated via mode-locked laser, which have enabled significantly advancement in precision optical frequency synthesis, optical clock, and metrology [1-4]. The comb source from mode-locked lasers usually have very low repetition rate like several hundreds MHz. The other kind of comb is generated based on electro-optic modulation of a continuous-wave laser with a series of intensity and phase modulators. This kind of comb usually has high repetition rate like 10 GHz. It is particularly desirable for applications [5], such as multi-wavelength coherent communication [6-8], optical arbitrary waveform generation [9-11], generation of low-phase noise [12], or agile ultrabraodband microwave [13], and RF signal processing [6,14]. Throughout this dissertation, we are mainly interested in the second kind of comb generated via electro-optic modulation at high repetition rate (10 GHz) for our RF photonic filtering application.

1.2. RF filters and RF photonic filters

Figure 1.2 shows an example of periodic RF filtering response [17]. Three attributes of an RF filter are (i) Free spectrum range (FSR), which is inversely proportional to the tap delay T; (ii) Mainlobe-to-sidelobe suppression ratio (MSSR); (iii) RF bandwidth. A high quality tunable RF filters should at least have the following functions:

(a) tunable RF filtering passband within a large range.

(b) Large MSSR (at least >30 dB, great with 60 dB level).

(c) RF bandwidth reconfigurability.

Tremendous efforts have been made attempting to achieve such goals by means of designing sophisticated RF circuits (or we call RF filters). In recent years, realizing such goals by means of optics technology (we call it RF photonic filters) has received

significant interests. In following sections, we will briefly overview and compare both RF filtering and RF photonic filtering technologies.

1.2.1. RF filters

Dramatic efforts have been done to implement kinds of RF tunable filters. For example, the introduction of Micro-Electro-Mechanical Systems (MEMS) variable capacitor approaches has led to recent advances in tunable RF filters [18-20]. The fundamental tuning speed of RF MEMS devices is characterized in [18] as limited to approximately 1-300 μs. Filters based on solid-state diodes have fundamentally higher tuning speeds but suffer from increased nonlinearity, loss, and power consumption [18]. Other filters under extensive investigations include Yttrium Iron Garnet (YIG) filters [21], Barium Strontium Titanate (BST) filters [22], tunable high temperature superconductor (HTS) filters [23], tunable dielectric resonator filters [24], micromechanical tunable filters [25], etc. However, for all above RF filtering technology, achieving large RF frequency tuning range with fast tuning speed (for example, for tens of nanosecond speed), demonstrating rapid bandwidth reconfiguration (for example, for tens of nanosecond speed), realizing very large mainlobe-to-sidelobe suppression ratio and stopband rejection are still very challenging.

1.2.2. RF photonic filters

RF photonics has demonstrated great advantages over the conventional RF technology such as RF signal (modulated on the optical signals) transmission over farther distances due to the low loss property of optical fibers, immunity to electromagnetic interference, higher operating RF frequency, and simpler reconfigurability [26-28]. By means of photonic technology, many challenges in RF signal processing may be easier to overcome when translated into optical domain due to normally huge optical operation bandwidth. For example, bandwidth reconfigurable RF filters are particularly useful for application such as cognitive radio, in which the radio can be tuned adaptively for the usage of free RF spectrum [29,30]. Although reconfiguring the RF bandwidth over a large faction by means of RF filtering technology is difficult, it is much easier to handle it after converted to the optical domain as we will discuss in Chapter 4.

A heavily discussed approach for RF photonic filters has a tapped delay line structure [26-28] as shown in Figure 1.3. Tapped delay lines yield finite impulse response (FIR) filters characterized by the zeroes of the response function [33], which are very flexible for configuring both phase and amplitude responses [34,35]. This scheme starts with multiple CW lasers with different frequencies. Controlling the power of each CW lasers is needed in order to adjust the weight of each tap. After combination, the signal goes through an MZM, with RF signal modulated on the optical carriers. Going through a dispersive element, each optical carrier experiences a frequency dependent delay. Then after the photodiode, the optical signal can be converted to electrical signal which is the RF output after filtering. One disadvantage of this scheme is that it is challenging to reach a large number of RF taps by combining a lot of CW lasers. Also adjusting the weight accurately of each taps by changing the optical power of each CW laser source is very challenging [14].

For N-tap microwave photonic filtering, the RF impulse response *h(t)* and frequency response *H(ω)* can be written as [14]:

$$h(t) \propto \sum_{n=0}^{N-1} \left|e_n\right|^2 \, \delta\left(t - nT\right) \qquad \text{and} \qquad H(\omega) \propto \sum_{n=0}^{N-1} \left|e_n\right|^2 e^{-jn\omega T} \tag{1.2}$$

where e_n is the electric field amplitude of the n^{th} tap, and $T = 2\pi\Delta f \psi_2$ is the differential delay between comb lines, determined by the group delay dispersion ψ_2 and the frequency spacing between comb lines Δf. From (1.2) the RF filter has a periodic frequency response with an FSR of T^{-1} and passband shape governed by the Fourier transform of the input tap power intensity [14].

Instead of starting with multiple wavelength CW lasers, recent efforts have been made to exploit broad light sources such as mode-locked lasers [36] or spliced continuous-wave incoherent light [37] to scale the number of RF taps with a single light source and a single dispersive element. However, the tuning of passband frequency tuning is challenging, which also suffers from reduced noise characteristics [38] (comparing with exploiting coherent multi-wavelength source) and dispersion induced distortion arose from the finite spectral width of sliced incoherent light source.

1.3. Brief introduction of comb-based RF photonic filtering approach

Different from the regular delayed tap line scheme based on multiple CW lasers or incoherent broadband source, in [14] our group demonstrated an approach for photonic implementation of RF electrical filters based on electro-optically generated frequency combs apodized using a programmable pulse shaper, which is capable of generating arbitrary optical ultrafast waveforms or power spectra according to user specification [39]. In [14]. a roughly flat optical frequency comb with repetition rate (comb line spacing) Δf ~10 GHz is generated by periodic intensity and phase modulation of a continuous wave (CW) laser via intensity and phase modulators [15-16]. A programmable pulse shaper is used to apodize the comb to Gaussian shaped. The apodized Gaussian-shaped comb is then passed through a single sideband modulator driven by the RF signal that we wish to filter. This places an identical sideband onto each of the optical comb lines. Then the signal propagates through a dispersive fiber and is then converted back to the RF domain using a photodetector. The comb lines arrive at the photodetector with different delays and hence function as independent taps in a tapped delay line filter architecture. The optical output signal, after being amplified by an EDFA is detected by a 22 GHz bandwidth photodiode and measured by a vector network analyzer over a span of 300 kHz – 20 GHz. The FSR of the filter can be adjusted with different length of DCF filter as dispersive element [14]. Our comb-based RF photonic filters have center frequencies and FSRs in the GHz range and bandwidths of hundreds of MHz, suitable for channelization of RF spectra at resolution matched to electronic analog-to-digital converter technology.

Figure 1.4 shows our scheme of an optical frequency comb based RF photonic filter. Our RF photonic filters were constructed using a single sideband modulator, a length of dispersion compensating fiber (DCF), and a 20-GHz bandwidth photodetector. The DCF fiber has specified dispersion of -1259.54 ps/nm at 1550 nm and relative dispersion slope (the ratio of dispersion slope to dispersion at 1550 nm) of 0.00455/nm. RF connections were made with conventional coax cables with specified 18 GHz bandwidth. Single sideband modulation is achieved using a dual drive lithium niobate Mach-Zehnder modulator, which may be viewed as an interferometer with independent phase

modulators in its two arms [40]. By driving the phase modulators with 90° RF phase shift and biasing the interferometer at 90° optical phase shift, all but one of the modulation sidebands can be canceled, leaving just a single sideband on each comb line. Our dual drive modulator has a half-wave voltage of 4.5 V at 1 kHz and a 3-dB bandwidth of 12.2 GHz. The phase shift between the RF drive signals is provided by a 90° hybrid splitter with a bandwidth of 1–12.4 GHz and a maximum phase imbalance of 7°.

Obviously, the advantages of this technique are:

- It uses only one CW laser source.
- Employing an optical frequency comb leads to a large number of taps.
- Novel tuning scheme based on variable optical delay in an interferometric structure.

The disadvantages of this technique are:

- A pulse shaper is needed so that the experimental setup is complex.
- The RF bandwidth of the filter is not reconfigurable.
- The resulting MSSR is limited to ~35 dB level due to the apodization accuracy of the line-by-line pulse shaper (0.37 dB ripple in the apodized spectrum) [14].
- The tuning speed of RF filter frequency is low by replacing the fiber in the interferometric structure

1.4. Dissertation outline

In the following chapters we will introduce several new concepts in comb-based RF photonics that bring special advantages for filter shape and tunability. The potential to implement highly selective filters which may be simply tuned in the nanosecond regime with rapid bandwidth reconfiguration offers a combination which appears not to be available from other approaches.

- Demonstration of high repetition rate flat-topped and Gaussian-shaped optical frequency comb generation. (Chapter 2)

- With directly generated Gaussian shaped comb based on electro-optical modulation technique, our RF photonic filter has 40 dB MSSR. Without the need for a pulse shaper, the experiment setup is greatly simplified. (Chapter 3)
- Demonstration of RF photonic filtering with 20 ns bandwidth reconfiguration. (Chapter 4)
- Demonstration of RF photonic filtering with enhanced enhanced MSSR at very rare 61 dB level. (Chapter 5)
- Demonstration of RF photonic filtering with 40 ns passband frequency tunability. A highlight in our approach is that filter lineshape is in principle independent of filter passband frequency tuning, which substantially eases control complexity. (Chapter 6)
- A summary of the accomplished results with some suggestions on future research directions. (Chapter 7)

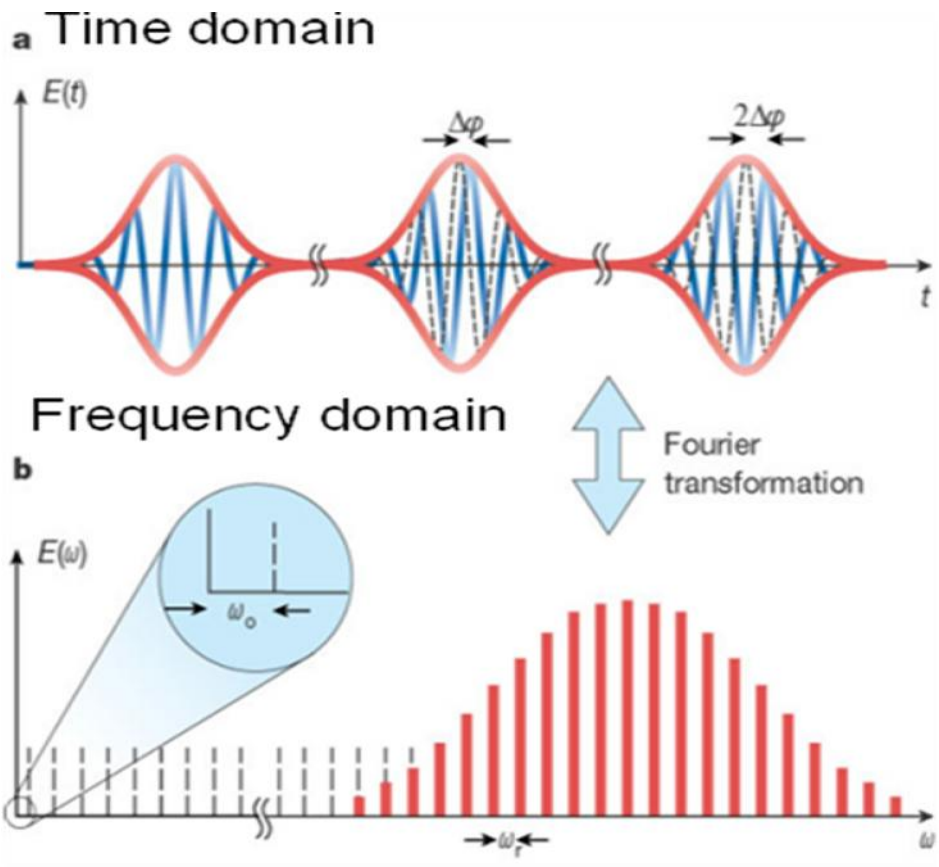

Fig. 1.1 Cartoon example of an optical frequency comb. (a) time domain (b) frequency domain (adapted from [1])

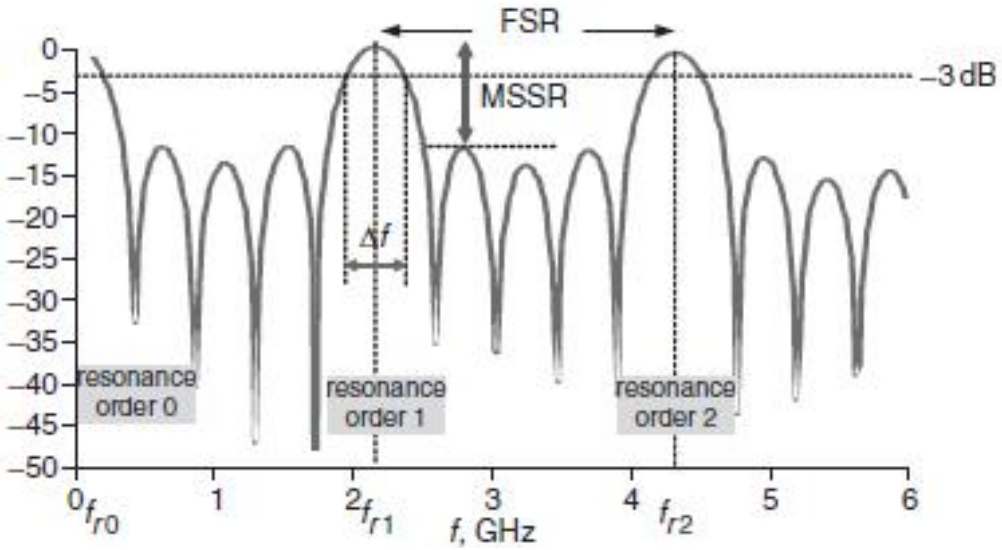

Fig. 1.2. A periodic multitap RF photonic filtering response (adapted from [17])

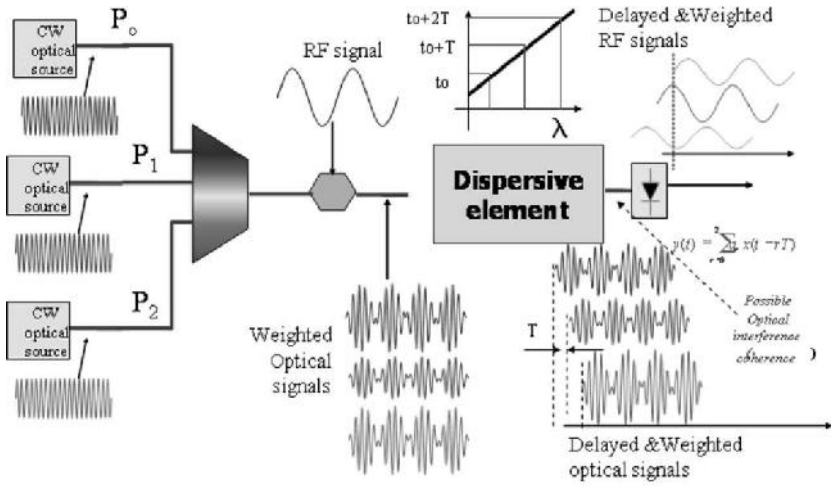

Fig. 1.3. A regular RF photonic filtering scheme based on multiple CW lasers (adapted from [17])

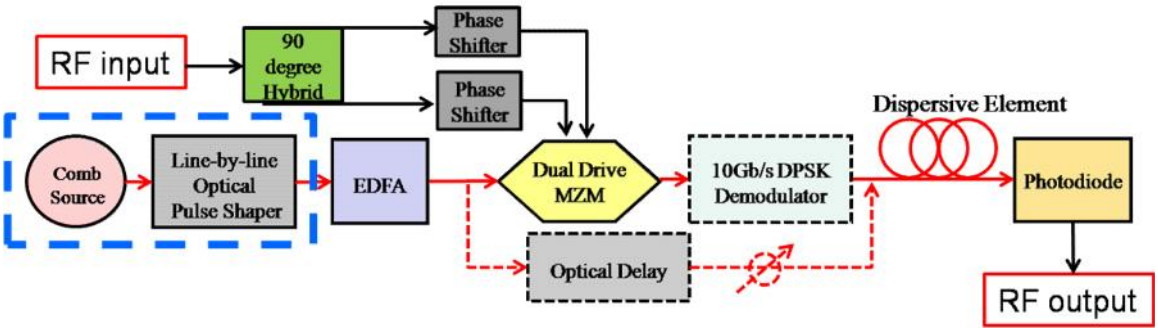

Fig. 1.4. Configuration of comb-based RF photonic filter (solid only: fixed filter configuration; with dashed components: tunable filter configuration). (adapted from [14])

2. HIGH REPETITION RATE PHASE MODULATED OPTICAL FREQUENCY COMB GENERATION

Optical frequency combs with a high degree of coherence, excellent spectral flatness, stability, as well as a broad bandwidth at high repetition rates are desirable for various applications such as wavelength division multiplexing [8], optical arbitrary waveform generation [9] and RF signal processing [41]. High repetition rate optical frequency combs with flat-topped or Gaussian-shaped are particularly interesting for these applications. Although tremendous efforts have been made to generate flat-topped optical frequency combs, current combs show either limited flatness (e.g., 61 lines within 7.4 dB variation [42]) or limited number of lines in the flat region (e.g., 11 lines within 1.1 dB variation [43] or 11 lines within 1.9 dB variation [44]). Additionally, so far very little work has been done to directly generate Gaussian-shaped optical combs. Hisatake et al demonstrated Gaussian-shaped comb generation based on spatial convolution of a slit and a periodically moving optical spot in a system based on electro-optic deflectors [45]. Here using only intensity modulators (IM) and phase modulators (PM), we present a novel 10-GHz dual-shape optical frequency comb generator without the need for a line-by-line pulse shaper. Our comb can be switched between extremely flat-topped (38 lines within 1-dB variation) and Gaussian (37 lines well matched to a Gaussian over 20-dB dynamic range), simply by turning on or off the RF amplifier to a single IM [16] [46]. To further broaden the comb bandwidth, we launch the Gaussian pulse generated from Gaussian comb into a length of highly nonlinear fiber (HNLF) with normal dispersion and generate a 10-GHz ultra-broadband flat-topped optical frequency comb (> 3.64-THz or 28 nm bandwidth with ~365 spectral lines within 3.5-dB power variation) covering the entire C-band [47].

*Most of this chapter has been published in [16,46,47]. I acknowledge collaborations and discussions with Dr. Christopher Long, Dr. V.R. Supradeepa, Dr. Victor Torres-Company, Dr. Daniel Leaird, and Prof. Andrew Weiner.

2.1. Flat-topped and Gaussian dual-shape optical frequency comb generator

2.1.1. Theoretical analysis

The shaped comb generation mechanism is based on time-to-frequency mapping theory, where quadratic and periodic temporal phase causes the spectral envelope to mimic the input intensity profile to the phase modulators [48-50]. In order to generate a flat-topped or Gaussian-shaped comb, the following two requirements should be met:

(i)Apply a quadratic phase.

Applying a purely quadratic, periodic temporal phase is difficult, so here we apply a "quasi-quadratic" phase by combining the first and second harmonic of the sinusoidal drive signal with power ratio 24-dB and phase shift 180° selected to suppress the 4^{th} order term of the cosine expansion of the phase shown in eq. (2.1). This substantially improves the approximation to the target quadratic phase profile.

$$\cos(\mu_m t) - \frac{1}{16}\cos(2\mu_m t) = \frac{15}{16} - 0.75\frac{(\mu_m t)^2}{2!} + 0 + \ldots \qquad (2.1)$$

(ii) Generate a flat-topped or Gaussian-shaped pulse.

We can use three intensity modulators (IM1, IM2, and IM3) to achieve this goal. IM1 and IM2 are both biased at 0.5 Vπ with RF drive amplitude 0.5 Vπ. IM3 is biased at 0 (maximum transmission) with RF drive amplitude Vπ in our simulation. We can get a flat-topped pulse with a series combination of IM1 and IM2 and a very close approximation to a Gaussian pulse with the series combination of all three IMs as shown in Fig. 2.1(a-b). After applying the quasi-quadratic phase as described in (i), we expect to obtain flat-topped and Gaussian combs as shown in Fig. 2.1(c-d), respectively.

2.1.2. Experimental setup

Fig. 2.2 shows the experimental setup of the 10-GHz Gaussian-shaped comb generator, which consists of three intensity modulators (IMs) and two phase modulators (PMs). We operate the RF oscillator at 10 GHz. At 10 GHz, the Vπ is ~9 V (~29 dBm) for the IM's and ~3 V for the PM's. The RF voltages delivered to IM1 and IM2 are both 0.5 Vπ zero to peak (~23.5 dBm), and the RF voltage to IM3 is Vπ. We cascade two

phase modulators at their maximum RF input power (30 dBm) to double the total modulation index seen by the pulse and increase the number of comb lines.

2.1.3. Experimental results

Fig. 2.2 (b-c) shows the experimental results. Without the black dashed module in Fig. 2.2(a) (equivalent to turning off RF amplifier TA3), we see a 10 GHz flat-topped comb spectrum with 38 lines within 1-dB variation [16] and 61 lines in total (Fig. 2.2(b)). This is a substantial improvement compared to previous published results. Fig. 2.2(c) shows the measured power spectrum of a Gaussian comb on a log scale. The standard deviation of the comb line amplitudes from a best-fit Gaussian profile is 0.42 dB for the central 37 lines and 0.26 dB for the central 35 lines, with an excellent match over 37 spectral lines across a -20 dB dynamic range [46].

2.1.4. Short pulse compression with flat comb

As a final demonstration of the quality of the generated comb, we compensate the residual quadratic phase in order to generate a short temporal pulse using only SMF. This scheme allows for excellent phase compensation with just a SMF link because the frequency comb has a strong quadratic phase character in time [16]. Fig. 2.3 shows the generated short pulse after compensating the chirp of the frequency comb with ~850 m of SMF. We see an excellent agreement between the experimental short pulse intensity autocorrelation and simulation. The autocorrelation FWHM of the obtained pulse is 2.8 ps, yielding a 2.1 ps FWHM assuming a sinc pulse shape, and a de-convolution factor of 0.75; the FWHM bandwidth of the comb spectrum is 391 GHz and the time-bandwidth product is 0.82 indicating compression close to the ideal transform limit of 0.884 for a sinc pulse shape.

2.1.5. Short pulse compression with Gaussian comb

Our Gaussian-shaped optical frequency comb is suitable for generation of trains of high quality picosecond pulses. Figure 2.4(a) shows the Gaussian-shaped optical frequency comb spectrum on a linear scale; again the shape agrees very well with the Gaussian fit. Figure 2.4(b) shows the spectral phase of the comb (blue) measured using a linear optical

implementation of spectral shearing interferometry [51]. The phase has a quadratic nature (red), as expected. This indicates pulse compression can be accomplished using the appropriate length of single-mode fiber (SMF). In order to characterize the pulses, we perform the autocorrelation measurement. The procedural is as follows: we amplified the pulses with an EDFA followed by a bandpass filter with 4 nm bandwidth programmed with the Finisar waveshaper in order to reduce the amplified spontaneous emission (ASE) noise. Then we launch the pulses to an autocorrelator for intensity autocorrelation measurement. The blue solid curve in Fig. 2.4(c) shows on a linear scale the measured intensity autocorrelation of the output pulse after passing the comb in Fig. 2.4(a) through 740 meter of SMF. The theoretical intensity autocorrelation (red dashed curve) taking into account the measured comb spectrum and assuming a flat phase is plotted as well. The excellent agreement between the two curves indicates high-quality pulse compression to the bandwidth-limit duration. The measured autocorrelation trace has 4.35 ps FWHM, corresponding to a 3.1 ps pulse width assuming a Gaussian pulse shape. Figure 2.4(d) shows the experimental intensity autocorrelation trace on a log scale. The autocorrelation trace shows a 22-dB dynamic range with respect to the background.

2.2. Supercontinuum-based flat-topped optical frequency comb generation

Prior investigations in spectral broadening of high-rep-rate temporal pulse trains from actively mode-locked lasers [52-56] or electro-optic frequency comb generator [57] showed a high degree of flatness with broad bandwidth when sech [53,54], parabolic [54,55] or Gaussian [56,57] profile pulses are launched into an HNLF operating in the normal dispersion regime. However, achieving this kind of temporal pulse shapes directly (i.e., without optical pre-shaping [39,58-59]) from an electro-optic frequency comb generator has remained challenging. Recently, we have shown the synthesis of a Gaussian-shaped comb [46] using the concepts of time-to-frequency mapping [48-50]. Here, we show that the temporal profile emerging from this comb can be used as a seed to achieve an ultra-broad optical spectrum (> 3.64-THz or 28-nm) with excellent flatness (more than 365 lines within 3.5 dB power variation) and a high-degree of coherence. To

illustrate the high-degree of stability and coherence of the source, we demonstrate pulse compression to the transform-limited duration.

2.2.1. System setup and results

Figure 2.5 shows the system setup to generate super-continuum flat-topped optical comb and the application for high-quality short-pulse compression. The whole setup is composed of three subsystems as follows:

The first part of Figure 1 explains our Gaussian-shaped comb generation scheme [46] as discussed earlier.

We note that to scale the scheme presented here to substantially beyond the current 10 GHz repetition rate raises practical challenges, both because of the need for the frequency doubler circuit itself and because the phase modulators must have a bandwidth equal to twice the repetition frequency. Our group has recently demonstrated similar improvements in the comb spectrum by exploiting four-wave-mixing in HNLFs and achieved ultraflat [60] or Gaussian-like [41] optical frequency comb generators without the use of a frequency doubler. These related schemes may be better suited for scaling to higher repetition rates. The 10 GHz repetition rate demonstrated here is already sufficiently high for application to comb-based RF photonics amplitude [46] and phase [61-62] filters.

Next, in order to perform spectral broadening, the transform-limited Gaussian pulse was amplified with an Er-Yb-doped optical fiber amplifier (OFA) and fed into 150 meters of HNLF with dispersion -1.88 ps/nm/km (as specified by the manufacturer), nonlinear coefficient of 10 (W·km)-1 and fiber attenuation of 0.22 dB/km as shown in the second part of Figure 2.5. Figure 2.6 shows our simulation results from solving the nonlinear Schrödinger equation using the split-step Fourier method [63]. For a qualitative study, we simulate the initial input pulse as a single perfect Gaussian-shaped profile with 3-ps FWHM as shown in black dotted trace of Fig. 2.6(a). The blue trace in Fig. 2.6(a) shows the output broadened pulse. Figure 2.6(b) shows the simulated output comb spectrum envelope (blue) and phase (red) with quadratic fit (black). The spectral phase has a quadratic profile within the turning points of the shoulders of the comb spectrum.

From a practical perspective, a specific length of SMF can be used to compensate for most of the spectral phase. Figure 2.7 shows the experimental output ultra-broadband flat-topped optical frequency comb spectrum when we tune the power of the OFA to 1.7 Watt. This comb shows excellent broadening and a flatness corresponding to 3.5 dB variation over 3.64 THz (28 nm or 365 lines), similar to the simulation prediction in Fig. 3(b). The characteristics of this comb source are promising for the realization of high-performance microwave photonic filters [41], where the ultimate limit in the achievable time-bandwidth product is directly proportional to the number of comb lines. This supercontinuum comb has already been demonstrated to be a promising source for such applications, with excellent stability in spectral amplitude, a large number of comb lines, and a broad bandwidth contributing to programmable microwave photonic phase filters with record time-bandwidth product [62]. We note that regions of the simulated intensity profile of Fig. 2.6(a) exhibit a nearly vertical rise or fall. Furthermore, the simulated and experimental spectra, Figs. 2.6(b) and 2.7, respectively, show clear spectral sidelobes on either side of the flat-topped central region. These observations are indicators that the pulse has entered into the wave-breaking regime [63-65]. This nonlinear phenomenon has been exploited as a route to achieve smooth and broad spectra with a high degree of stability [64] when pumped with bell-shaped pulses, and is gaining increasing popularity for applications requiring high-quality ultrashort-pulse compression [66]. Our experiments indicate that this phenomenon can also take place in the high-repetition-rate regime and is indeed suitable for applications involving electro-optic frequency comb generators. We have also performed measurements – at a lower average power level (0.75 W) – to test the stability of the comb. Figure 2.8 (a) shows the simulated optical spectrum (blue) with spectral phase (black) and quadratic fit (red) at 0.75 W average power. Comparing with the simulated comb spectrum at 1.7 W average power in Fig. 2.8(b), the comb bandwidth in Fig 2.8(a) is somewhat decreased due to the reduced pump power. We repeatedly measured the comb spectrum using an OSA set for 0.01 nm spectral resolution, recording 14 spectra over a period of approximately 70 minutes. The output comb spectrum has 237 lines (18.6 nm or 2.36 THz) within 4.5 dB power variation as shown in Fig 2.8(b). Figure 2.8(c) provides data on the stability of each of the

individual comb lines over this data set. Most of the comb lines have variations with standard deviation below 0.1 dB. The average and median standard deviations of all the comb line variations are 0.08 dB and 0.09 dB, respectively. The largest fluctuations are observed for the four lines closest to the input CW laser (1542 nm), with a standard deviation ranging from 0.35 dB to 0.66 dB. Overall, this indicates the stability of this comb source can be very good.

2.2.2. Application for short pulse compression

Maintaining a high degree of coherence across the entire bandwidth of the supercontinuum obtained by picosecond pump pulses is challenging [52]. According to a previous study, the situation improves when the HNLF is designed to have a normal dispersion profile [67], since the amplification of input noise due to modulation instability is avoided. Thus, apart from offering a smooth and broad spectrum, an HNLF with normal dispersion should provide a supercontinuum with high degree of coherence too. In order to demonstrate the high quality of our broadened comb as well as the spectral stability, I perform a pulse compression experiment. The broad supercontinuum was attenuated by 10-dB and sent to a commercial pulse shaper (FinisarWaveshaper 1000S), as indicated in Fig. 2.5. The output from the shaper was measured with an autocorrelation apparatus. When the pulse shaper was programmed as an all-pass filter, the autocorrelation trace has a roughly triangular shape, much broader than the initial Gaussian pulse [black dotted trace in Fig. 2.9(a)] before the HNLF. The approximately triangular autocorrelation is roughly as expected for the flat-topped intensity profile predicted in the nonlinear wave-breaking regime in Fig 2.6. The slight narrowing of the experimental autocorrelation trace (Fig. 2.9(a)) relative to the simulated one (Fig 2.6(a)) is attributed to the dispersion in the short SMF between HNLF and the pulse shaper. From Fig. 2.6(b), one can conclude that the central part of the spectrum can be easily compensated for by introducing the right amount of dispersion. In order to compensate for the comb phase, we first programmed the pulse shaper to apply the amount of quadratic spectral phase that maximized the second-harmonic generation (SHG) at the zero delay position of the autocorrelation setup. Figure 2.9(b) shows the measured

autocorrelation trace (blue) with very large pedestal. Similar to what was observed in [54], the measured trace does not match the calculated autocorrelation based on the input comb spectrum assuming a flat phase. An explanation is that the outer part of the spectrum, as shown in the simulation of Fig. 2.6(b), deviates from quadratic phase. To overcome this limitation, I programmed the pulse shaper to apply a spectral window [68] that selects the central 20 nm of the supercontinuum comb as shown in Fig. 2.7. In this region the phase remains approximately quadratic and the spectrum maintains an approximately rectangular profile. Again we programmed the pulse shaper to apply the amount of quadratic spectral phase that maximized the SHG at the zero delay position. The autocorrelation now shows a high-quality pedestal-free trace as shown in the blue curve of Figure 2.9(c), which has an excellent correspondence with the calculated one taking into account the measured spectrum after windowing and assuming a flat spectral phase. The ability to achieve pulse compression to the transform-limit indicates a high degree of coherence across the comb spectrum –i.e., the relative phase of the different comb lines do not vary significantly in time [69]. The autocorrelation width is 533 fs FWHM. To estimate the actual pulse width, we calculate the transform-limited intensity profile and estimated its width to be 490 fs FWHM, as shown in Fig. 2.9(d).

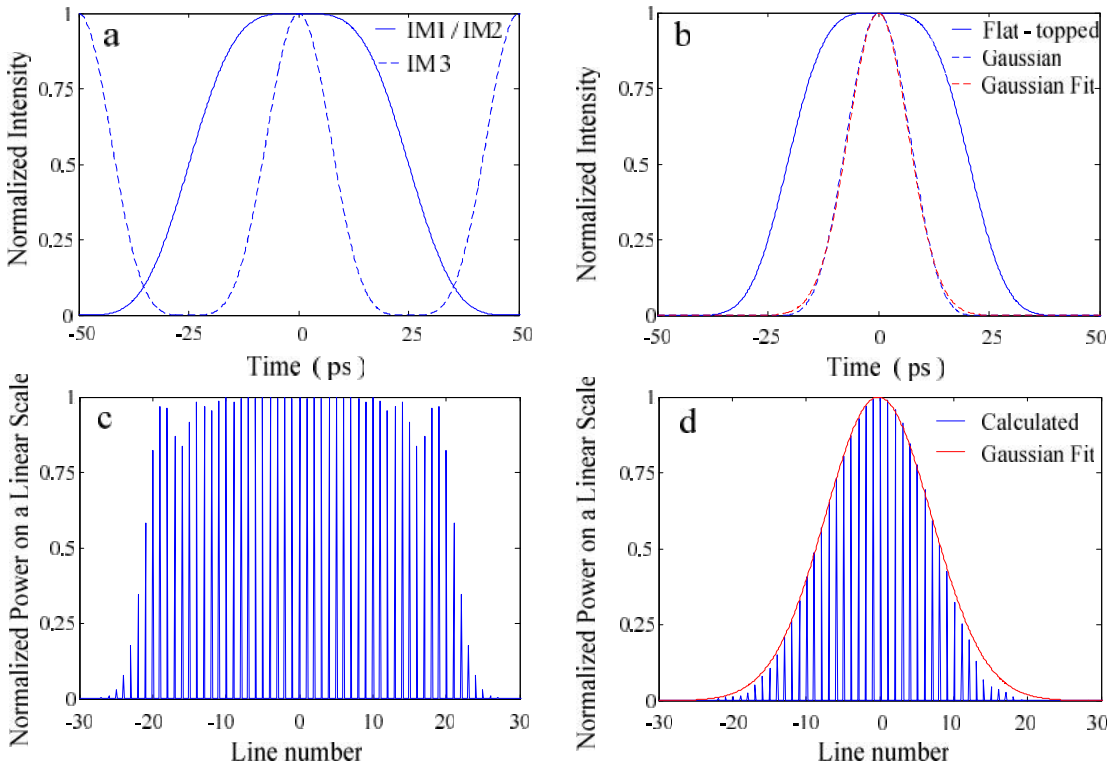

Fig. 2.1. Simulation results: (a) Solid: transmission function from IM1 or IM2; Dashed: transmission function from IM3 (b) Solid blue: flat-topped pulse expected from series combination of IM1 and IM2; Dashed blue: Gaussian pulse expected from the series combination of IM1, IM2 and IM3; Dashed red: Gaussian fit (c) Simulated flat-topped comb spectrum (d) Simulated Gaussian-shaped comb spectrum

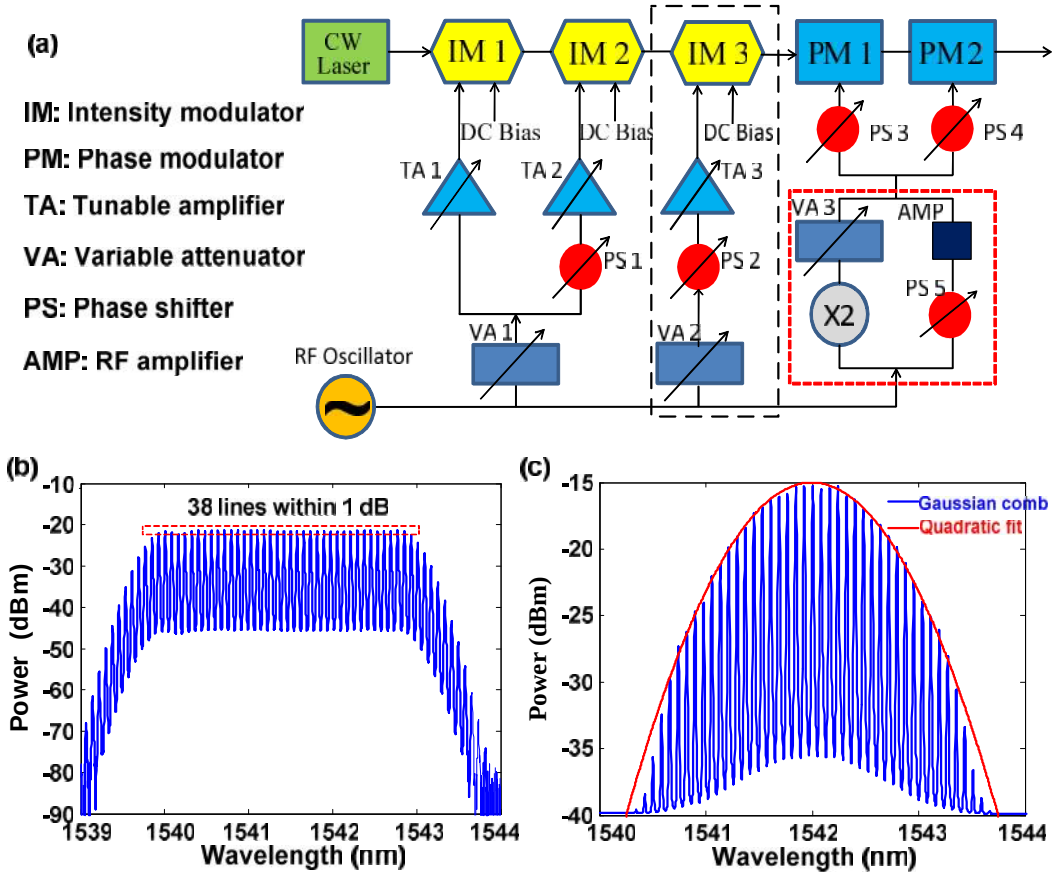

Fig. 2.2. Experiment (a) setup for flat-top and Gaussian dual-shape optical frequency comb generator (b) Experimental result of flat-topped comb (c) Experimental result of Gaussian shaped comb

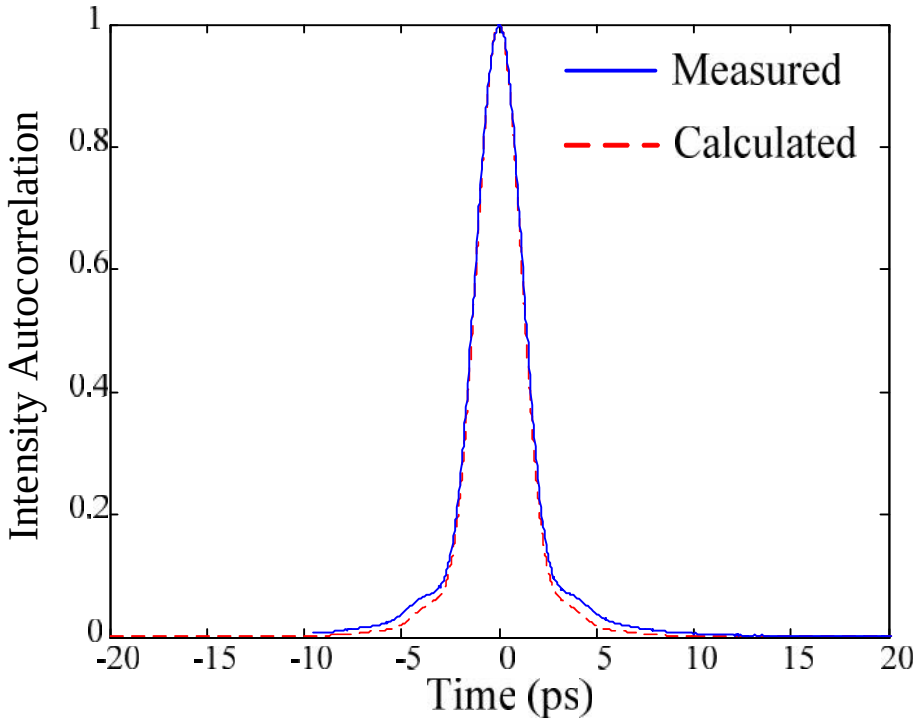

Figure 2.3. High quality short pulse generation with the flat comb

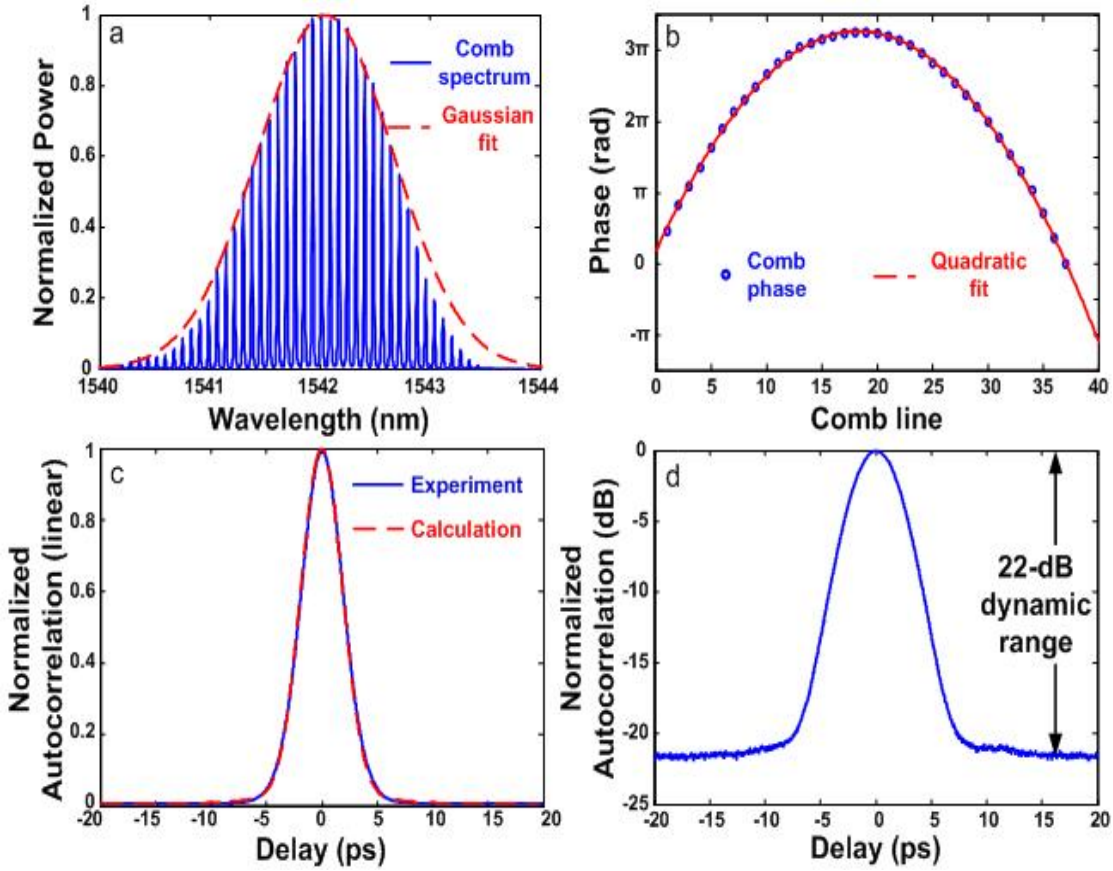

Fig. 2.4. Experimental results: (a) Gaussian-shaped comb on a linear scale (blue) and Gaussian fit (red); (b) Measured spectral phase (blue) and quadratic fit (red); (c) time domain intensity autocorrelations of the output pulse obtained after comb propagates through ~740 m of SMF (blue) and calculated autocorrelation trace taking the comb spectrum (a) and assuming a flat spectral phase (red). An excellent agreement is seen between the two; (d) Experimental intensity autocorrelation on a log scale which shows 22 dB dynamic range.

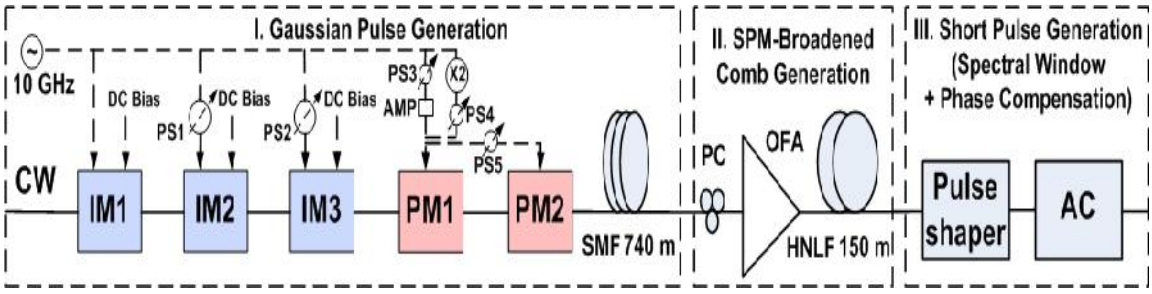

Fig. 2.5. Experimental scheme to generate supercontinuum flat-topped comb and the application for high quality temporal pulse compression. CW: continuous wave; IM: intensity modulator; PM: phase modulator; PS: phase shifter; AMP: RF amplifier; SMF: single-mode fibers; PC: polarization controller; OFA: Er-Yb-doped optical fiber amplifier; HNLF: highly nonlinear fiber; AC: autocorrelator.

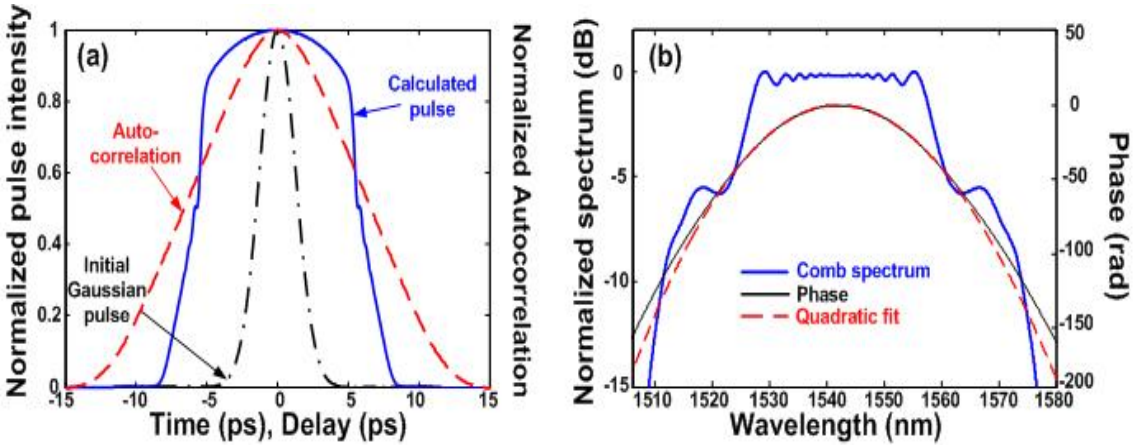

Fig. 2.6. Simulation results (a) Propagating Gaussian pulse in 150 m HNLF with 1.7 W average power. Initial pulse with 3-ps FWHM (black), output pulse (blue) and corresponding autocorrelation trace (red); (b) Output optical spectrum envelope (blue) and phase (black) with quadratic fit (red).

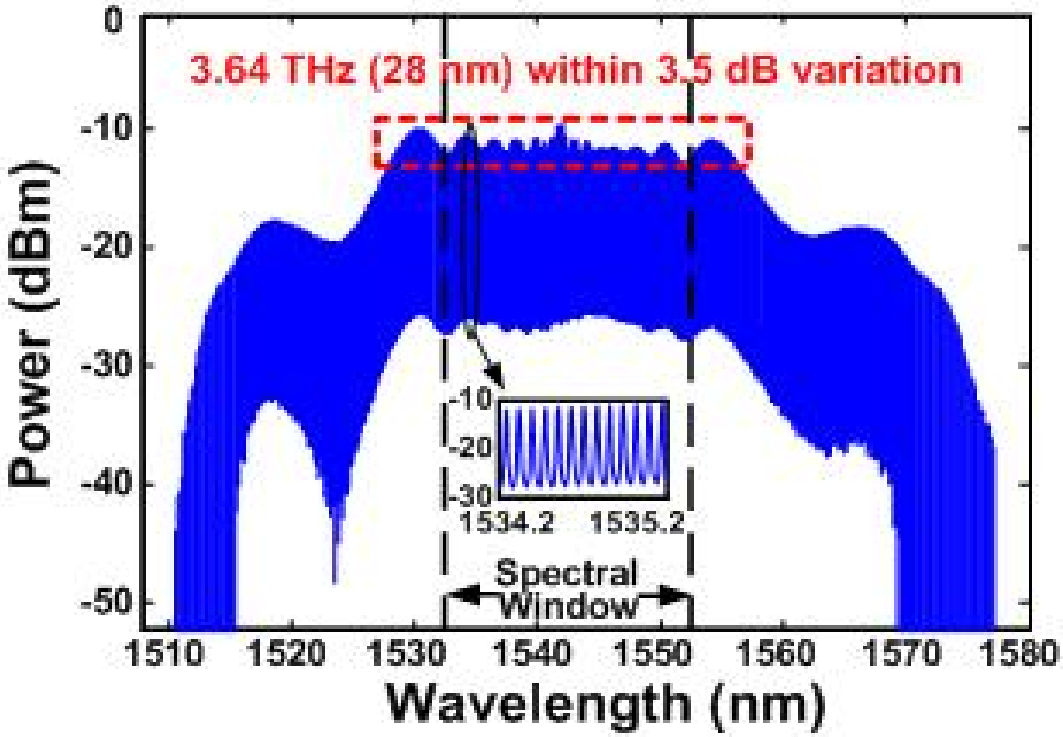

Fig. 2.7. Experimental optical power spectrum after propagation in 150-m HNLF with 1.7-W pulse average power before HNLF measured with 0.01nm OSA resolution. A spectral window, equivalent to a bandpass filter, keeps the center spectrum with linear chirp.

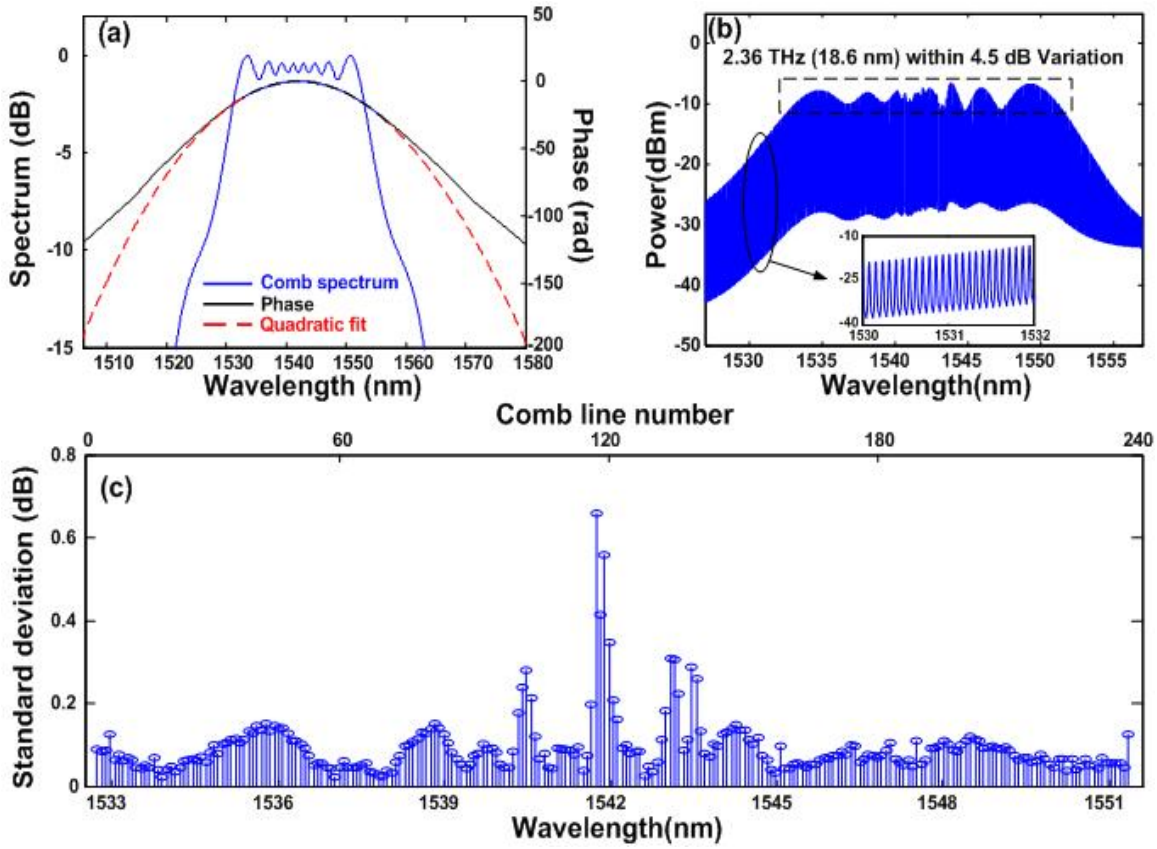

Fig. 2.8. Stability analysis: (a) Simulated optical spectrum (blue) with spectral phase (black) and quadratic fit (red) at 0.75 W average power. (b) Optical spectrum measured with 0.01nm OSA resolution. (c) Stability analysis which shows spectral amplitude standard deviation of each comb line versus the number of comb line and wavelength after approximately 70 minutes of measurements.

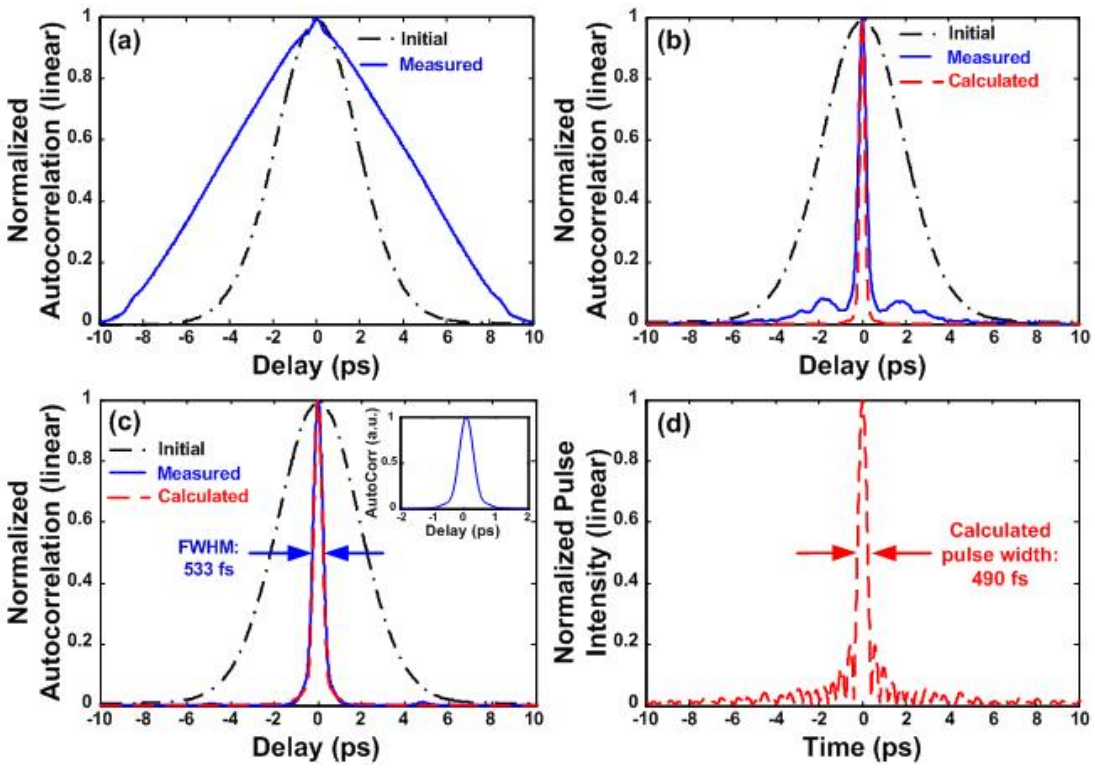

Fig. 2.9. Application of the flat-topped super-continuum comb for short pulse compression. Measured autocorrelation traces of the initial Gaussian pulse, after compression, at the output of the first box in Fig. 1 shown as black traces in (a)-(c)); (a) Blue trace: measured autocorrelation trace of pulse with the whole spectrum of super-continuum comb without phase compensation; (b) blue trace: measured autocorrelation trace of pulses with the whole spectrum of super-continuum comb after quadratic phase compensation; red trace: calculated autocorrelation trace with the input super-continuum comb assuming a flat phase; (c) blue trace: measured autocorrelation trace of pulse with the truncated spectrum of super-continuum comb after quadratic phase compensation; red trace: calculated autocorrelation trace with the truncated super-continuum comb assuming a flat phase. An excellent agreement between the experimental and simulated autocorrelation traces indicates accurate spectral phase compensation. Inset is the zoom-in of measured pulse autocorrelation trace. The corresponding pulse shape is calculated in (d).

3. RF PHOTONIC FILTERING WITH DIRECTLY GENERATED SHAPED OPTICAL FREQUENCY COMB

Using an optical frequency comb as a multiple carrier optical source offers new potential for achieving complex and tunable RF photonic filters. For applications in RF photonic filtering, a carefully apodized Gaussian comb is preferred in order to achieve clean passband shapes with large sidelobe suppression. Reference [14] used line-by-line pulse shaping to manipulate the amplitudes of individual spectral lines to obtain a carefully apodized Gaussian shape for achieving clean passband shape with 35 dB sidelobe suppression, and also demonstrated a novel mechanism that allows tuning of the filter largely independent of passband shape. Starting with a comb designed to have a Gaussian-shape resulting directly from the generation process is another interesting choice. Here by employing the Gaussian-shaped comb discussed in the previous chapter, we implement filters with 40 dB MSSR suppression. The results are improved over that reported in [14] (~35 dB).

3.1. The effect of comb shape on the final filter shape

Before we introduce our scheme, let us make a brief discussion and analyze the effect of comb shape on the final filter shape based on the theoretical transfer function eq. (1.2).

We assume the comb source spacing equals to 10 GHz with a total of 50 lines. We choose the length of dispersion compensation fiber such that we can obtain 100 ps delay spacing between adjacent taps and the center frequency of the filter response is 10 GHz.

If we start a flat-top comb as plotted in figure 3.1(a), the resulting filter has a shape of sinc function with only about 13.3 dB MSSR in figure 3.1(d) as plotted in blue. If we apodize the comb source by a Gaussian profile with 190 GHz 3-dB bandwidth as plotted in figure 3.1(b), the resulting filter has a shape of Gaussian with about 58 dB MSSR in

*Most of this chapter has been published in [41,46]. I acknowledge the discussions with Prof. Andrew Weiner.

figure 3.1(d) as plotted in black. If we future narrow the Gaussian comb into one with 130 GHz 3-dB bandwidth as plotted in figure 3.1(c), the resulting filter MSSR is increased significantly to about 115 dB in figure 3.1(d) as plotted in red. From this simulation study, we observe have two observations:

(1) Filter shape depends on the comb shape. Gaussian comb is desirable for achieving high contrast filter.

(2) Starting with narrow bandwidth Gaussian shaped comb (truncated to zero level) helps to achieve high contrast filter shape.

3.2. RF photonic filtering with directly generated Gaussian shaped comb

For experimental demonstrations, we generate 10 GHz flat-topped and Gaussian-shaped optical frequency comb based on setup shown in Figure 2.2. First, we turn off TA3 (in Fig. 2.2). Fig. 3.2(a) shows a 50-line 10-GHz flat-topped optical frequency comb spectrum measured at the photodiode (in fixed filter setup of Fig. 1.4). After turning on TA3, Fig. 3.2(b) shows a 41-line 10-GHz Gaussian-shaped optical frequency comb spectrum measured at the photodiode; the EDFA is adjusted to set the average power at the photodiode to 4.3 dBm, as used with the flat-topped comb. The standard deviation of the comb line amplitudes from a best-fit Gaussian profile is 0.42 dB for the central 37 lines and 0.26 dB for the central 35 lines, with an excellent match over 37 spectral lines across a 20-dB dynamic range. Comb spectra were measured using a monochromator-based optical spectrum analyzer (OSA) with 0.01 nm resolution.

After applying the comb to our filter setup, we measured the filter transfer function with a vector network analyzer, usually set for 10 Hz resolution bandwidth. We compare our experimental results, adjusted an RF calibration factor which accounts for high frequency roll-off due to cable loss and modulator and photodiode frequency response, with simulation. The RF calibration data can be obtained by measuring the link frequency response without the dispersion compensating fiber [4]. This takes out RF frequency dependences due to cable loss and high frequency component roll-off, thereby focusing on the RF response intrinsically related to our photonic processing scheme [14]. Fig. 3.2(c) shows the measured (blue, after calibration) and simulated (red) filter transfer functions using the flat-topped comb. At baseband, the filter has a 3-dB bandwidth of 116

MHz, with 16.2 dB MSSR. The passband at 10.4 GHz has a 3-dB bandwidth of 255 MHz with 14.2 dB MSSR. Modeling (based on the measured optical power spectrum) indicates the filter has a 3-dB bandwidth of 130 MHz and 262 MHz with 15.8 dB MSSR at both baseband and passband, in very close agreements with our experiment. Fig. 3.2(d) shows the measured (blue) and simulated (red) filter transfer functions using the above Gaussian-shaped comb. At the baseband, the filter has a 3-dB bandwidth of 186 MHz, with 40 dB MSSR. The 10.4 GHz passband has a 3-dB bandwidth of 355 MHz with 33.7 dB MSSR. Modeling indicates the filter has a 3-dB bandwidth of 210 MHz and 420 MHz with 36.6 dB MSSR at both baseband and passband, in very close agreements with our experiment. The filter FSR is determined by the length of DCF fiber. By adding or decreasing the length of DCF we can change FSR, and vary the filter pass band center frequency accordingly.

Because of the periodic nature of discrete-time filters, unwanted higher-order mixing terms may also be generated by this filter. For instance, an optical sideband may mix with a neighboring comb line to produce a signal that is located in a higher frequency band. As discussed in detail elsewhere [14], a variety of tones at frequencies $m\Delta f$ and $m\Delta f \pm f_{RF}$ may be present at the output, where f_{RF} is the frequency of a single RF input tone, Δf is the comb spacing, and m is an integer. In order to avoid aliasing related to such effects, sampling theory restricts operation of digital filters to an upper frequency of one half of the sampling frequency. In the case of an optical comb-based RF photonic filter, this sampling rate corresponds to the comb repetition rate Δf. Note that in a network analyzer measurement, which is based on coherent mixing with a reference tone, only a signal with frequency equal to that transmitted from the network analyzer is acquired; other output tones are not detected. Nevertheless, in order to avoid spurious output tones, the frequency span should be restricted to fall within a single "Nyquist zone," where the various Nyquist zones run from $p\Delta f/2$ through $(p+1)\Delta f/2$, where p is a nonnegative integer. For figures in which the filter response is plotted over a range exceeding $\Delta f/2$, the boundaries between Nyquist zones are depicted as dashed vertical lines, similar to [14]. The free spectral range (FSR) of our filters may be adjusted though choice of the fiber dispersion. For the data of Figs. 3.2 (c) and (d), due the length of available fiber,

the filter FSRs fall close to 10 GHz, which is the boundary between second and third Nyquist zones [41].

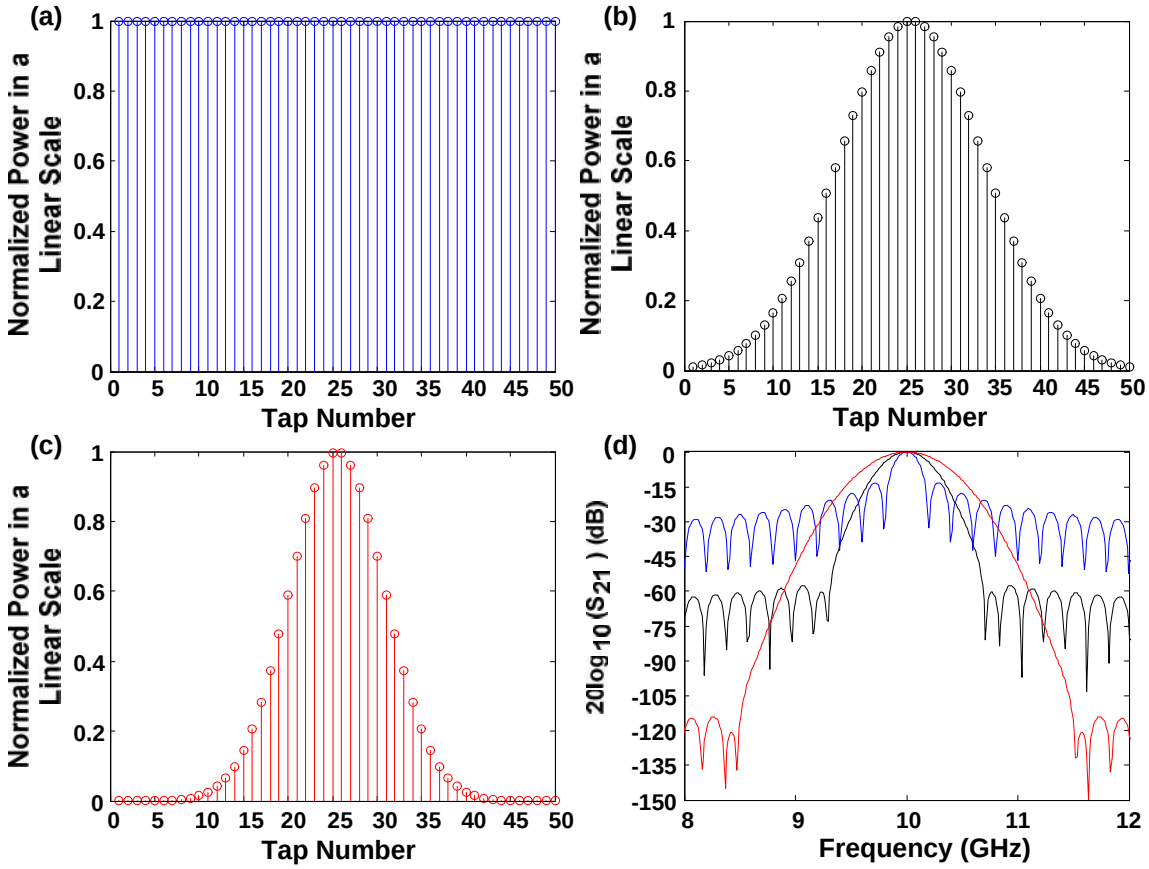

Fig. 3.1. Simulation (a) Flat comb (b) Gaussian apodized comb with 3-dB bandwidth of 190 GHz. (c) Gaussian apodized comb with 3-dB bandwidth of 130 GHz. (d) Simulated filter transfer functions for combs of (a, blue), (b, black) and (c, red) respectively.

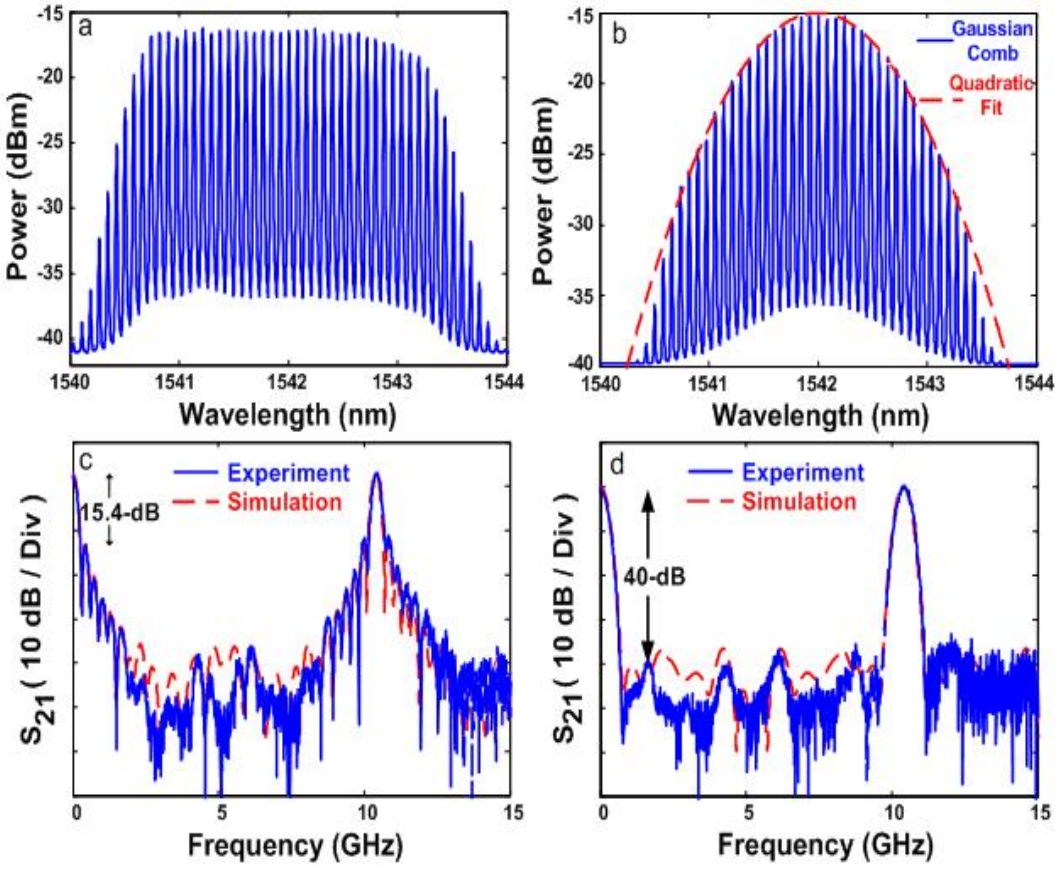

Fig. 3.2. Experimental results: (a) Flat-topped comb on a log scale; (b) Gaussian-shaped comb on a log scale; (c) Measured (blue) and simulated (red, after calibration) RF photonic filter transfer functions with flat-topped comb in (a); (d) Measured (blue, after calibration) and simulated (red) RF photonic filter functions with Gaussian-shaped comb in (b).

4. RF PHOTONIC FILTERING WITH 20 NS BANDWIDTH RECONFIGURATION

Rapid bandwidth reconfiguration of the RF photonic filter is of great interest. Although many efforts are made toward implementation bandwidth reconfigurable filters based on RF circuits [70-77], the relevant research focuses on improving filter parameters such as decreasing insertion loss, shrinking the size of the device, increasing the range of bandwidth reconfigurations, etc. For example, [70] demonstrates bandwidth reconfiguration of up to 33% for the filters with less than 3 dB insersion loss with a commercially available low Q varactors (Q < 30). However, rapid RF bandwidth reconfiguration (for example, at the level of tens of nanosecond), to the best of our knowledge has not been demonstrated. Here we demonstrate rapidly changing the bandwidth of an optical frequency comb through the use of an electronically programmable RF variable attenuator; RF bandwidth reconfiguration of the filter has been demonstrated with 20-ns reconfiguration speed while keeping the mainlobe-to-sidelobe suppression ratio (MSSR) larger than 30-dB. The reconfiguration speed is determined by the response time of the RF variable attenuator.

4.1. Experimental setup

Figure 4.1 shows the experimental setup for the RF bandwidth reconfigurable filters. The dotted part is the bandwidth tunable optical frequency comb generator, which is a sequence of lithium niobate electro-optic intensity and phase modulators. The modulator sequence is designed to generate an approximately Gaussian-shaped optical comb spectrum [41,46] based on time-to-frequency mapping theory [48-50]. We fix the RF power on one phase modulator to 30 dBm, while the RF power on the other phase modulator is also 30 dBm when the variable attenuator is turned off. The variable attenuator provides approximately 23 dB attenuation when switched “ON”. The comb bandwidth is proportional to the modulation index on the phase modulators [16]. So the comb optical bandwidth is expected to reconfigure accordingly to the

*I acknowledge the discussions with Dr. Daniel Leaird, and Prof. Andrew Weiner.

RF power change on the phase modulator through the control of the RF variable attenuator. For filtering applications, the generated comb is modulated according to a single-sideband modulation. Then the signal passes through a dispersion-compensating fiber (DCF) and is detected by a photodetector. Each line of the optical frequency comb acts as a distinct filter tap, with tap delay set by the comb spacing and the dispersion.

Eq. (1.2) indicates that the RF bandwidth varies inversely proportional with the bandwidth of the optical frequency comb, which is in turn proportional to the modulation index to the phase modulators.

4.2. Simulation studies

Figure 4.2 shows an example of simulation results. Figure 4.2(a) and (b) show Gaussian apodized combs with 20 lines (102 GHz 3-dB bandwidth) and 36 lines (182 GHz 3-dB bandwidth), respectively. Since total optical power is not changed with phase modulation depth, the peak power of the comb in Figure 4.2(b) is reduced compared to the comb in Figure 4.2(a). Figure 4.2(c) shows the filter transfer functions in blue (corresponding to the comb in Figure 4.2(a)) and in red (corresponding to the comb in Figure 4.2(b)), respectively. Simulation indicates the filter peaks have the same heights for both cases. The 7.9 GHz passband has a 3-dB bandwidth of 513 MHz (blue) and 285 MHz (red), respectively. From blue to red, the RF bandwidth decreases by 44.4%.

4.3. Experimental demonstration

Figure 4.3 shows our measured optical spectrum (a,b) with optical spectrum analyzer (OSA), and RF filter transfer function (c) with vector network analyzer (VNA). By switching the variable attenuator from “ON” to “OFF”, the optical 3-dB bandwidth increases from 0.82 nm to 1.62 nm as shown in Figure 4.3(a) and (b). The resulting filter transfer function shown in Fig. 4.3(c) reveals a decrease in 3-dB bandwidth of the RF filter passband from 518 MHz to 272 MHz. The RF bandwidth decreases by 47.5% similar to that estimated in Figure 4.2(c).

We now demonstrate RF bandwidth reconfiguration of the filter by injecting two RF tones at 7.9 GHz and 8.4 GHz, at which frequency (marked in vertical lines in Fig. 4.3(c)) our filter exhibits different frequency response when switching the programmable attenuator. We intentionally set the power of 8.4 GHz RF input signal 8 dB larger than that of 7.9 GHz

waveform in order to equalize the RF output powers of both frequency tones when the attenuator is switched on as shown in Figure 4.4(a). The RF spectrum is measured using an RF spectrum analyzer. Figure 4.4(b) shows the corresponding oscilloscope trace of the filtered RF output when the attenuator is switched on, measured with a 50Gsample/s real-time oscilloscope. With similar power at both frequency tones. the RF waveform in Figure 4.4(b) exhibit periodic and oval-shaped envelope. Similarly when the attenuator is off, the output RF frequency tones with >10 dB power difference are shown in Fig. 4.4(c). Fig. 4.4(d) shows the corresponding oscilloscope trace of the filtered RF output. Since the RF power at 7.9 GHz dominates over that at 8.4 GHz, the periodic and oval-shaped envelopes of RF waveforms in Fig. 4.4(c) cannot be observed in Fig. 4.4(d). The contrasting RF spectra and waveforms when the attenuator is switched on and off clearly indicate the RF bandwidth reconfiguration of the filter.

Figure 4.5 demonstrates rapid RF bandwidth tuning by applying a rapidly varying ON/OFF control signal at 625 KHz modulation rate (1.6 μs period) to the variable attenuator. The oscilloscope trace of the filtered RF output is shown in Fig. 4.5(a). Close-up waveforms at different time sections are shown in Fig. 4.5(b) when the attenuator is switched off (same as Fig. 4.4(c)), and Fig. 4.5(c) when the attenuator is switched on (same as Fig. 4.4(a)). The contrasting character is clearly preserved. Figure 5(d) shows a spectrogram of the oscilloscope data in Figure 4.5(a) calculated using a sliding fast fourier transform hamming window of 41 ns duration, providing an intuitive visual representation of the filtering. Examination of the rapid transition at the rising and falling edges of the frequency bands at 8.4 GHz as shown in inset (e) and (f) reveals that the filter is able to switch within 20 ns, limited by the response time of the RF variable attenuator.

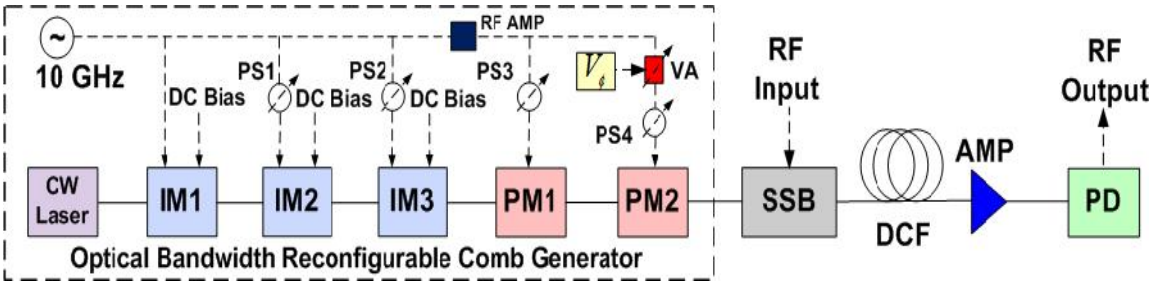

Fig.4.1. Experimental scheme to implement bandwidth reconfigurable RF photonics filtering based on optical bandwidth tunable optical frequency combs. CW: continuous wave, IM: intensity modulator, PM: phase modulator, PS: phase shifter, VA: RF variable attenuator, SSB: single sideband modulator, DCF: dispersion compensating fiber, AMP: optical amplifier, RF AMP: RF amplifier, PD: photodetector.

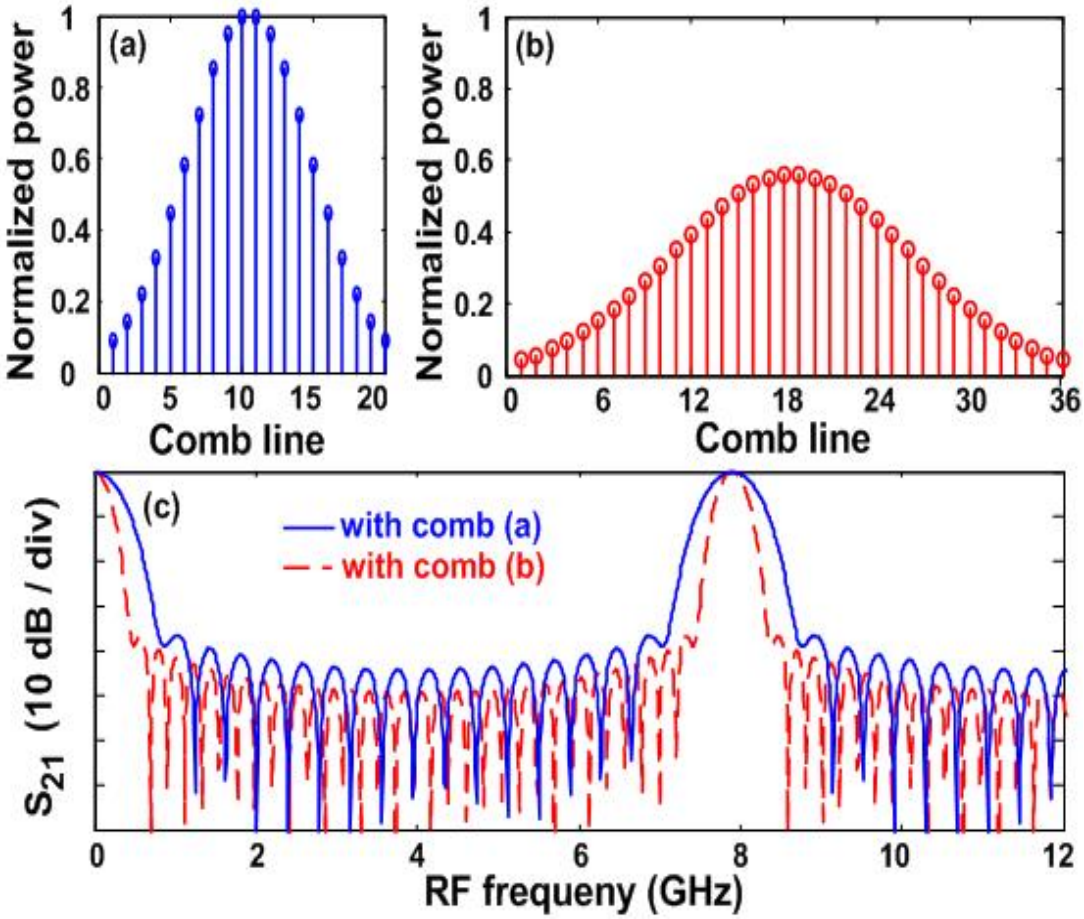

Fig. 4.2. Simulation results of bandwidth reconfigurable filter. (a) Optical frequency comb spectrum with 20 comb lines. (b) Optical frequency comb spectrum with 36 comb lines. (c) Calculated filter transfer functions with comb a and b respectively.

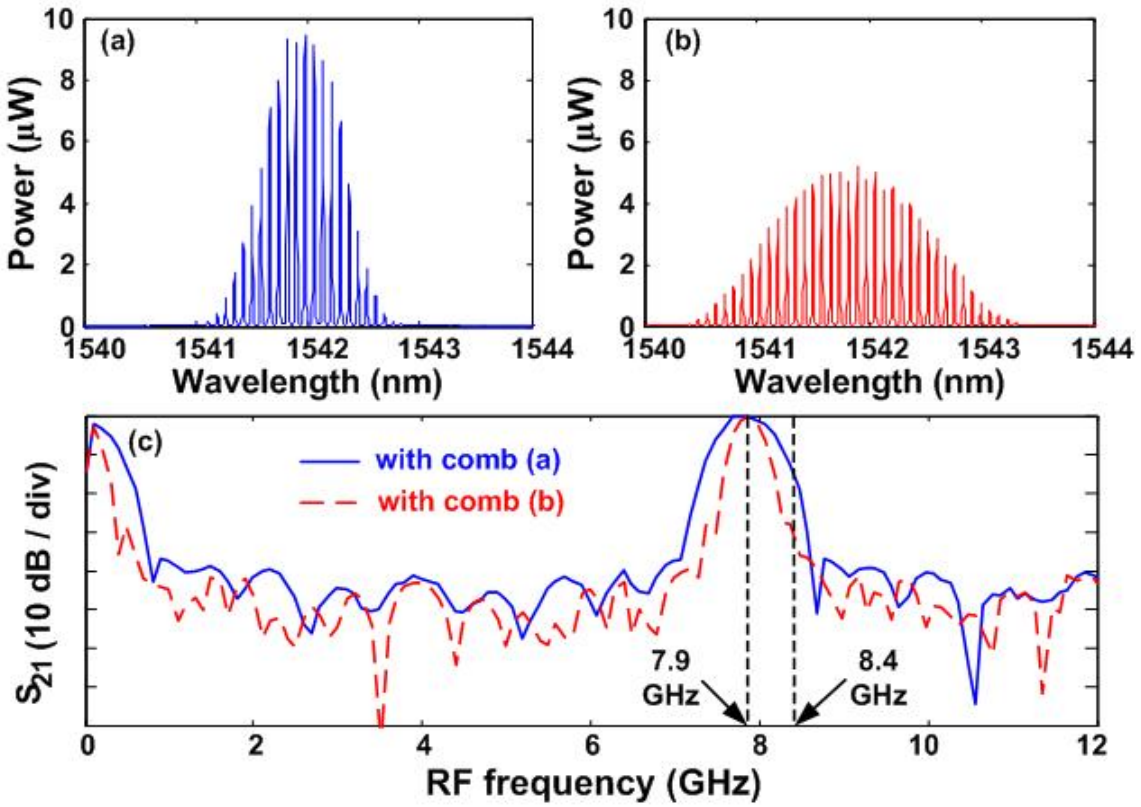

Fig. 4.3. Experimental results of the bandwidth reconfigurable RF photonic filtering through the use of a programmable RF variable attenuator. (a) Optical frequency comb spectrum with the variable attenuator switched "ON". (b) Optical frequency comb spectrum with the variable attenuator switched "OFF". (c) Measured RF filter transfer functions with comb a (attenuator switched "ON") and comb b (attenuator switched "OFF").

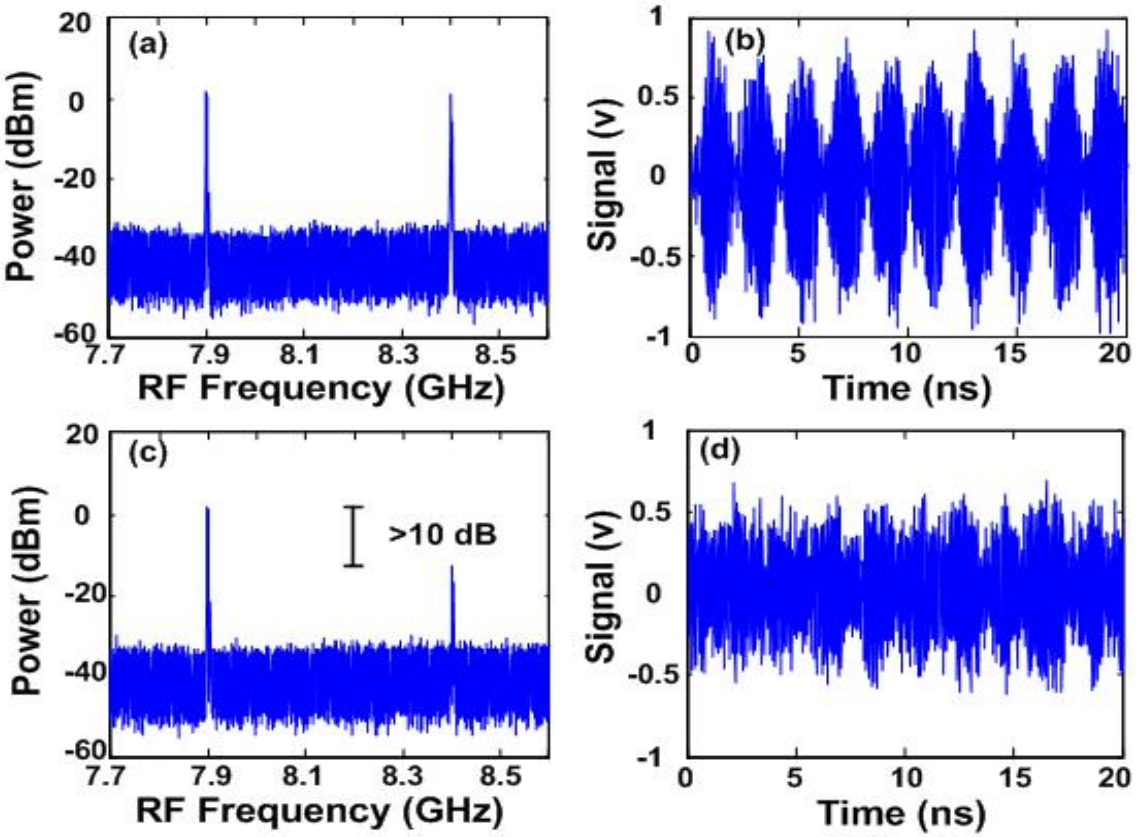

Fig. 4.4. Experimental RF output characterization of bandwidth reconfiguration in both time and frequency domain by switching the attenuator "ON" and "OFF". Switched "ON": (a) Output RF spectrum showing the two RF frequency tones at 7.9 GHz and 8.4 GHz have approximately equal power. (b) Output RF waveform measured with real-time scope. Switched "OFF": (c) Output RF spectrum showing the two RF frequency tones at 7.9 GHz and 8.4 GHz have >10 dB power difference. (d) Output RF waveform measured with real-time scope.

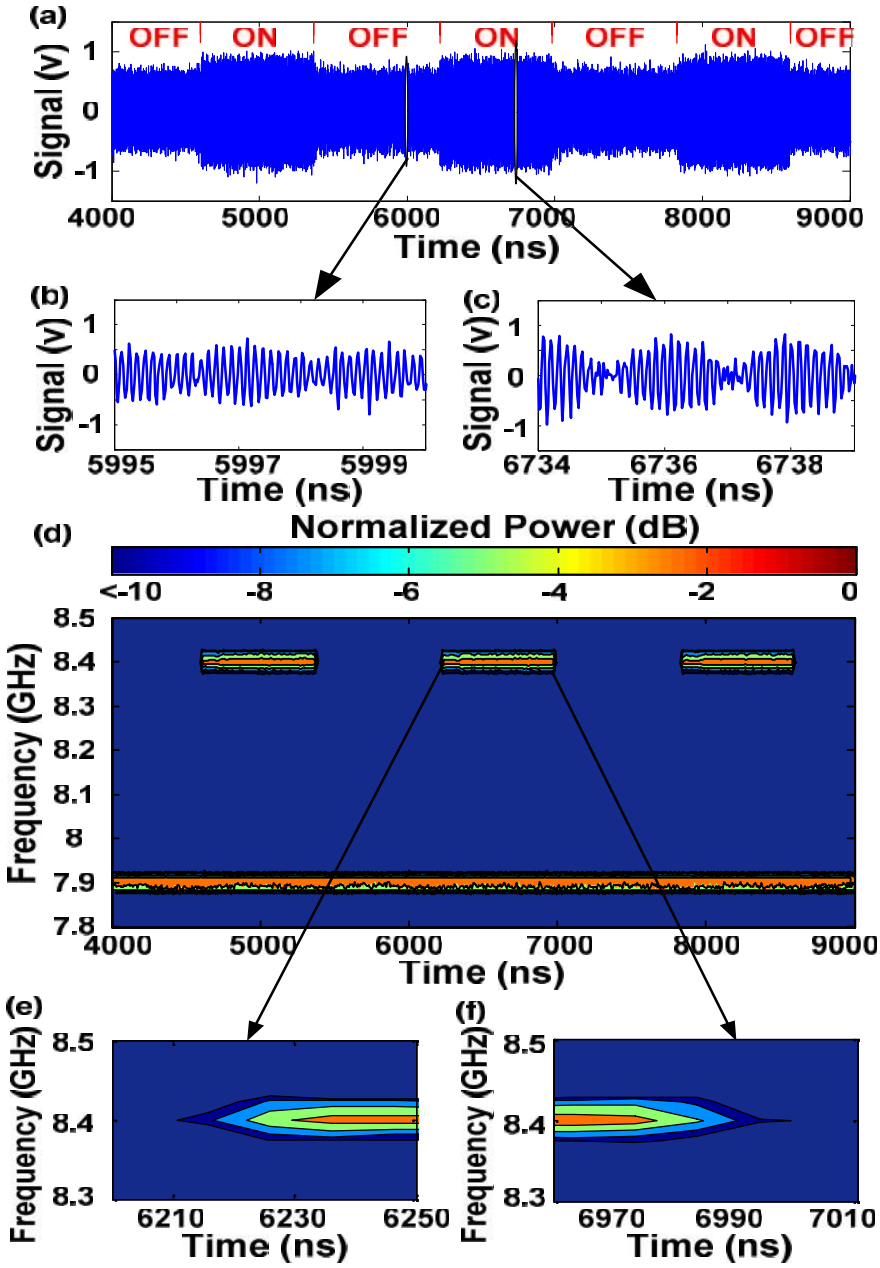

Fig. 4.5. Experimental results showing rapid RF bandwidth reconfigurability of the RF filter. a. Measured oscilloscope signal. b. Close-up of a first waveform part of the signal (attenuator "OFF"). c. Close-up of a second waveform part of the signal (attenuator "ON"). d. Spectrogram representation of the output filtered signal, highlighting rapid RF bandwidth reconfiguration. e. Close-up of the first spectrogram part at the rising edge. f. Close-up of the second spectrogram part at the falling edge.

5. RF PHOTONIC FILTERING WITH >60 DB MAINLOBE TO SIDELOBE SUPPRESSION RATIO

We now focus on enhancing the selectivity of the RF photonic filter, manifested through high MSSR and stopband attenuation. In the area of RF photonic filtering, the regular MSSR limits to 35 dB level [14,17,32,36]. Further increasing MSSR to >35 dB level has been very challenging. Recently, the use of a recirculating frequency shifter as a tapped delay line yielded filters with passbands centered in the 100-200 MHz range, free spectral range (FSR) of ~35 MHz, main-to-sidelobe suppression ratio (MSSR) of 52 dB, and stopband attenuation of >70 dB [78]. In another example, apparently based on a cascade of five coupled optical microresonators, a fifth-order filter with 70 dB stopband suppression [79] was reported.

The key to high selectivity in our scheme is to achieve an extremely smooth and specifically shaped comb spectrum with minimal line-to-line variations. Direct electro-optic generation of an approximately Gaussian comb, described above, is a first step, but substantial improvement in spectral shaping is still required. Here we introduce a dual-laser driven comb generator plus nonlinear fiber optics approach that simultaneously broadens and smoothes the comb spectrum to achieve selective filters with greatly enhanced MSSR and stopband attenuation. High efficiency conversion through four-wave mixing has been previously utilized for a variety of tasks in optical communications [80-81]. Here we utilize cascaded four-wave mixing as a phase modulation amplifier and spectral smoother. The resulting filtering response has MSSR of ~61 dB and stopband attenuation of >70 dB, comparable to the results mentioned above.

5.1. The effect of multiplicative noise on the filter MSSR

The key for achieving large MSSR is to employ an extremely smooth and specifically shaped comb spectrum with minimal line-to-line variation. Reference [14] tried to use a

*Most of this chapter has been published in [41]. I acknowledge collaborations and discussions with Dr. V.R. Supradeepa, and Prof. Andrew Weiner.

line-by-line pulse shaper to manipulate the amplitudes of individual spectral lines to obtain a Gaussian shape for this purpose. However, the MSSR was limited to the 35 dB level primarily by the precision with which the optical comb spectrum was apodized. With directly generated Gaussian-shaped comb, we increase the MSSR to 40 dB level. Here, we significantly improve the smoothness of the comb by combining nonlinear optics and electro-optic modulation comb generation schemes, which boosts the MSSR to >61 dB level. In this section, I will present a simulation study which highlights the effect of the smoothness of the comb spectrum on the MSSR of the resulting radio-frequency photonic filters.

Let us start with 50 comb lines (50 taps) perfectly shaped as a Gaussian with a full-width at half-maximum (FWHM) bandwidth equal to 13 times the comb spacing (e.g., 130 GHz optical bandwidth for 10 GHz comb spacing). We then assume the comb lines are subject to multiplicative noise following a normal distribution. Figure 5.1(a) shows both a perfect Gaussian comb (red) and an example of a comb subject to multiplicative noise with 0.2% standard deviation (blue). Figure 5.1(b) shows a perfect Gaussian comb (red) and an example of a comb subject to multiplicative noise with 5% standard deviation (black). This level of variation is roughly similar to that reported in [14], where the smoothness of the comb was limited both by spectral variations and drift arising from a less advanced electro-optic comb generation geometry and by pulse shaping precision. Figure 5.1(c) shows the RF photonic filtering responses predicted for the above comb spectra in a fixed filter geometry. Starting with a perfectly apodized Gaussian comb, we expect to get a filter with 115 dB MSSR (red), limited only by truncation of the Gaussian due to finite number of taps. With 0.2% standard deviation multiplicative noise, the MSSR decreases significantly to 60 dB (blue), similar to the experimental results shown later in red in Fig. 5.1(c). With 5% standard deviation multiplicative noise, the MSSR is reduced to 34 dB (black), similar to the experimental results reported in [14].

Clearly, a smooth comb spectrum is essential for achieving high contrast RF photonics filtering. In Fig. 5.1(d), we overlay 100 simulation results for each level of multiplicative noise (standard deviations of 0.2% and 5%, respectively). The overlaid simulation traces exhibit mainlobe-to-sidelobe suppression ratios similar to those shown in Fig. 5.1(c).

So an extremely smooth optical frequency comb is essential to achieve a comb-based RF photonic filter with a large MSSR. For a 50-tap Gaussian comb with 10 GHz comb spacing and 130 GHz FWHM bandwidth, we estimate multiplicative variations of the comb spectrum must remain below approximately 0.2% standard deviation to achieve a mainlobe-to-sidelobe suppression ratio of >60 dB

5.2. Experimental setup

Figure 5.2(a) shows the experimental setup for the quasi-Gaussian shaped comb generator inspired by [60]. As in Fig. 5.2(a), EO intensity and phase modulators produce a quasi-Gaussian spectrum on a CW laser centered at 1542 nm. A second CW laser (1532 nm) is combined without intensity modulation and passes through the same phase modulator. For reasons that will become clear, one comb is delayed with respect to the other by one half the modulation period (50 ps at 10 GHz). This is followed by an amplifier and zero dispersion, low dispersion slope highly nonlinear fiber (HNLF). Cascaded four wave mixing (FWM) in the HNLF leads to amplification of the phase modulation and substantial spectral broadening and smoothing. Figure 5.2(b) shows a schematic of the comb generation process. The initial two combs are narrow bandwidth and have poor spectral quality. As we look at successive FWM terms, the combs bandwidth scales while the spectral shape becomes more Gaussian.

To understand this process more quantitatively, let $a_1=|a_1(t)|\exp(j¤(t))$ be the complex amplitude of laser 1 (centered at f_1) which undergoes intensity and phase modulation. The intensity envelope $|a_1(t)|^2$ is shaped to look roughly Gaussian, and the temporal phase $¤(t)$ is sinusoidal. Laser 2 (centered at f_2) is only phase modulated, and its complex amplitude can be written as $a_2=\exp(j¤(t))$. After transmitting through a length of SMF which delays laser 2 by half a modulation period with respect to laser 1, the complex amplitude of laser 2 can be written as $a_2=\exp(-j¤(t))$. In the HNLF these waveforms mix to give a cascade of FWM terms. In the limit of negligible HNLF dispersion, the first FWM term centered at $(2f_1-f_2)$ will be primarily composed of

$$a_1^2 a_2^* = |a_1(t)|^2 \exp(j3¤(t)) \tag{5.1}$$

Similarly, the 2nd order FWM will go as

$$a_1^3 a_2^{2*} = |a_1(t)|^3 \exp(j5\phi(t)) \quad (5.2)$$

Equations (5.1) and (5.2) correspond to scaling of the bandwidth by three times and five times, respectively. Furthermore, since the temporal intensity profile becomes increasingly localized as it is raised to progressively higher powers, the temporal phase is increasingly well approximated as quadratic. This results in higher fidelity time-to-frequency mapping and increasingly smooth combs.

In the comb source of Fig. 5.2(a), the two CW lasers are spaced 10 nm apart. We operate the RF oscillator at 10 GHz, for which the V_π is ~9 V for the IM's and ~3 V for the PM's. IM1 is biased at quadrature with the RF amplitude of 0.5 V_π zero to peak. IM2 is biased at the maximum transmission point with the RF amplitude of V_π. The transmission function is $a_1 = 0.5[1+\exp(-j0.5\Phi)\exp(j0.5\Phi\cos(\mu_{RF}t))]$ for IM1, and $a_2 = 0.5[1+\exp(j\Phi\cos(\mu_{RF}t))]$ for IM2. The phase modulation $\phi(t)$ is from the single phase modulator, driven at its maximum RF input power (30 dBm) to maximize the modulation index seen by the gated pulses after IM2. The SMF used to delay one frequency with respect to the other by half a modulation period is ~300m. This is followed by a 1.5-W optical amplifier and a 100 m length of highly nonlinear fiber, with near zero dispersion and low dispersion slope, to create a cascade of four-wave mixing (FWM) terms. By use of a bandpass filter, we select the FWM term centered at 1562 nm.

5.3. Experimental results

Figures 5.3(a) and 5.3(b) show the comb spectrum of laser 1 right after the modulators and of the 2nd order FWM term, respectively. Both bandwidth enhancement and spectral smoothing are clearly seen. Figure 5.3(c) shows the corresponding filter transfer function measured using the network analyzer. The two measured filter functions have different FSRs due to the 20 nm red shift of the 2nd order FWM signal and the dispersion slope of the DCF module. The filter response (blue dashed line) for the comb shown in Fig. 5.3(a) has a peak at baseband with 3-dB bandwidth of 350 MHz, while at 10.4 GHz there is a passband with 800 MHz 3-dB bandwidth. The filter response (red solid line) for the comb shown in Fig. 5.3(b) has a peak at baseband with 3-dB

bandwidth of 210 MHz, while at 9.38 GHz (corresponding to 107.5-ps tap delay) there is a passband with 440 MHz 3-dB bandwidth. The roughly two-fold reduction in passband width is attributed to the increased comb bandwidth. Most importantly, the MSSR and stopband suppression are increased to 61 dB and >70 dB, respectively, the latter limited by the VNA noise floor. Simulations in 5.1 suggest that to reach these levels of performance, random variations of the comb spectrum must have standard deviation below ~0.2% (9×10^{-3} dB). Such variations are ~40 times smaller compared to previous results in which apodization of a comb is performed using a pulse shaper [14], leading to improvements in MSSR and stopband attenuation by >25 dB. The level of sidelobe suppression and stopband attenuation demonstrated here is extremely rare in RF photonics; to our knowledge comparable levels are reported only in [78] and [79].

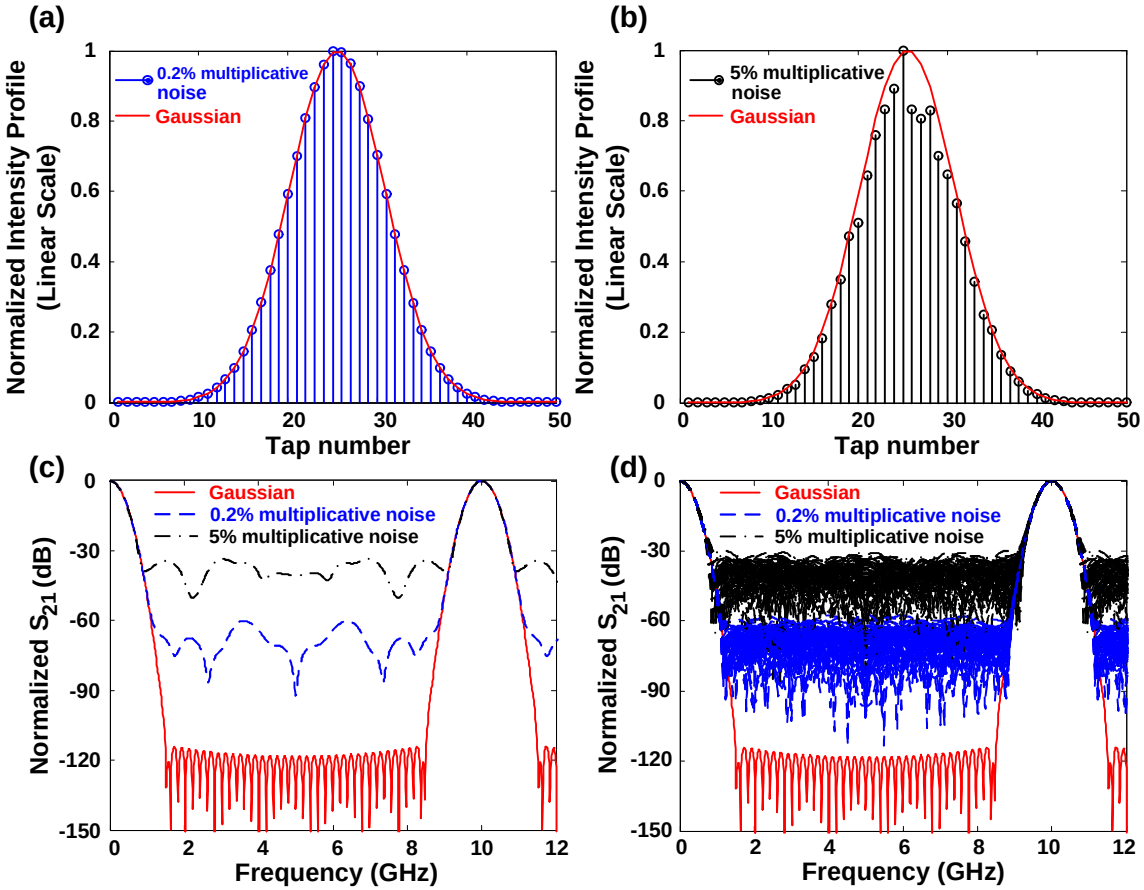

Fig. 5.1. Simulations illustrating the effect that random spectral variations of a Gaussian-apodized frequency comb have on resulting microwave photonics filters. Random spectral variations are modeled as multiplicative noise, and a delay of 100 ps per tap is assumed.

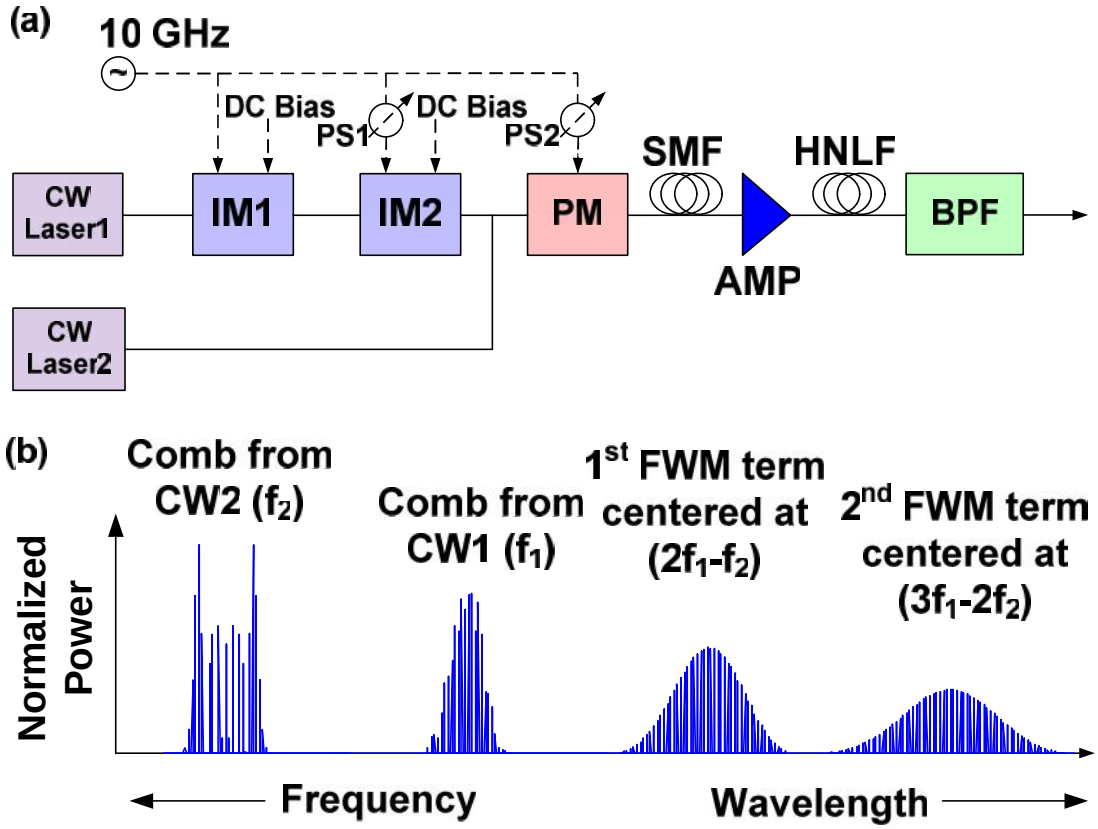

Fig. 5.2. Direct, high accuracy generation of Gaussian apodized broadband combs. a, Experimental scheme to directly generate broadband, apodized combs using cascaded four-wave mixing in highly nonlinear fiber. SMF – single mode fiber, HNLF – Highly nonlinear fiber. b, Depiction of the cascaded four-wave mixing process. Successive terms scale in bandwidth and correspond increasingly accurately to a smooth Gaussian apodization.

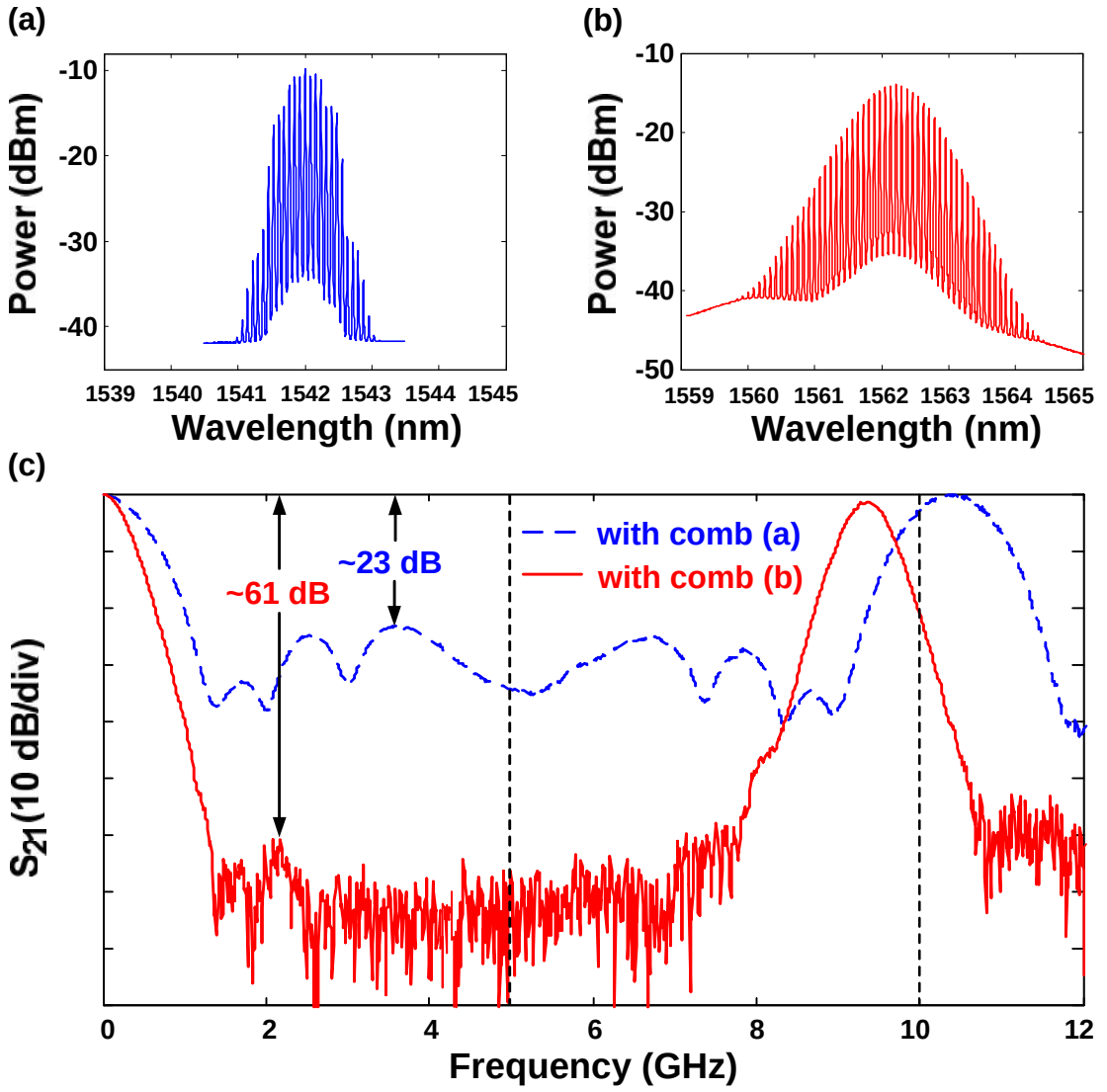

Fig. 5.3. Achieving high stop-band attenuation RF filters. a, Spectrum from laser CW1 measured directly after the modulators, b, Measured spectrum of the 2nd order cascaded FWM term used in our experiment. c, Measured RF filter transfer function using the 2nd order FWM term, Fig. 5.3(b), demonstrating extremely high main lobe to sidelobe suppression ratio (61 dB) and stop-band attenuation (>70 dB). Also shown is the measured transfer function using only the comb after the modulators, Fig. 5.3(a).

6. AGILE RF PHOTONIC FILTER WITH 40 NS TUNING SPEED

Although the passband frequency may be tuned by changing the amount of dispersion, this is inconvenient and not rapidly adjustable. Recently, our group proposed a new approach to achieve filter tuning with fixed dispersion [14], shown schematically in Fig. 1.4. This method utilizes an interferometric configuration in which one sample of the comb is single sideband modulated with the carrier suppressed, while a second sample of the comb remains unmodulated but experiences a tunable optical delay. The frequency response of the RF filter obtained after the two samples of the comb are combined, sent down a dispersive line, and detected can be written as [14]:

$$H(\mu) \propto \sum_{n=0}^{N-1} e_{1n} e_{2n}^{*} e^{-jnT(\mu - \mu_0)} \tag{6.1}$$

where e_{1n} and e_{2n} are the complex electric field amplitudes of the n^{th} comb line in the two arms of the interferometer and τ is the relative delay between the two optical paths. If e_{1n} and e_{2n} are from the same comb, their phases will cancel, again leading to tap amplitudes given by $|e_n|^2$, i.e., by the comb spectrum. Equation (6.1) shows that the center frequency of the filter can be controlled by the relative delay. This was demonstrated for the first time in [14], which used a mechanical delay line to achieve quasi-static tuning.

Rapid tuning of the RF filter response by tuning the laser frequency relative to the optical filter has been proposed [80]. However, rapidly (e.g., submicrosecond) controllable tuning of a CW laser over a range of a few GHz is itself a difficult challenge, and to the best of our knowledge, the use of this technique to realize rapid RF filter tuning has not been demonstrated. Achieving rapid tuning of the laser wavelength while maintaining the required wavelength control and coherence is the major challenge to this approach.

*Most of this chapter has been published in [41]. I acknowledge collaborations and discussions with Dr. Christopher Long, Dr. Fahmida Ferdous, Dr. Daniel Leaird, and Prof. Andrew Weiner.

Here we introduce a new scheme that exploits dual electro-optically generated frequency combs to achieve radically enhanced tuning speed. For our scheme, our tuning is based on optical delay, in principle independent of filter lineshape control.

6.1. Experimental setup

Fig. 6.1(a) shows our experimental setup for the rapid tuning filter. A single CW laser is split and directed into two nominally identical comb generators, each following the approach of Fig. 6.1(b). In each comb generation, three cascaded lithium niobate intensity modulators generate a train of 10-GHz pulses that are approximately Gaussian in time, to which we then apply a strong sinusoidal phase modulation. For pulsed signals centered at extrema of the sinusoid, the temporal phase is approximately quadratic, which results in time-to-frequency mapping, with the temporal intensity of the waveform mapped onto its power spectrum [48-50]. This time-to-frequency mapping enables direct generation of an approximately Gaussian frequency comb. Figure 6.1(c) shows the generated spectrum in this scheme. Our filter tuning experiments utilize a pair of nominally identical comb generators designed for approximately Gaussian spectra. From Eq. (6.1), the filter response is sensitive to the difference in the frequency dependent optical phase of the combs. Minimum filter bandwidth is obtained if the combs are identical so that their spectral phases cancel. Although simulations indicate that the filter shape is robust against minor differences in the drive conditions of the two comb generators, nevertheless, we attempt to generate two combs that are as close to identical as possible. The modulation indices on the phase modulators are matched by monitoring and comparing the individual optical spectra, and the indices of individual intensity modulators are set by monitoring their outputs on an RF spectrum analyzer as the bias conditions are changed. Next the RF phase (delay) between modulators is set by observing the comb with both RF and optical spectrum analyzers. By watching for certain key signatures (e.g., a minimized comb line or harmonic), it is possible to very accurately set the proper bias and delay conditions and make the two combs very similar in terms of amplitudes and phases.

Fig. 6.1(d) shows the frequency response of the RF photonic filter, measured using a vector network analyzer (VNA), and overlaid with a simulation based on Eq. (1.2) and the measured comb spectrum. As expected, we see two Gaussian-like passbands separated by the filter FSR. Fiber dispersion produces a tap delay of T = 96 ps and a corresponding FSR of 10.4 GHz. The passband centered at 10.4 GHz has a 3-dB bandwidth of 750 MHz, with stopband attenuation of over 28 dB. Overall the measured filter function is close to the simulated response based on the comb spectrum, with confirms the predicted Fourier transform relationship.

As above, one of the combs is single-sideband modulated (but now with suppressed carrier), while the other remains unmodulated but is provisioned with controllable delay. A key observation is that since the two comb generators are driven at the same RF frequency, the relative delay of the generated optical trains is governed by the relative phase shift of the respective RF drive signals. Analog RF phase shifters are available that can vary phase over a 2π range with >50 MHz modulation bandwidth. By utilizing such a phase shifter, the delay of the generated comb can be electronically tuned over a full comb period in tens of nanoseconds.

6.2. Experimental results

Figure 6.1(e) demonstrates rapid tuning of the optical delay between combs. The experiment is set up so that initially the two comb signals are overlapped in time (top panel). A step input to the control port of the RF phase shifter induces a change in the relative delay. As seen from the bottom panel, one of the optical pulse trains is shifted in this example by 20 ps (corresponding to ~20% of the comb repetition period) in < 30ns. This permits tuning of the RF filter response within a comparable time span, substantially faster than conventional RF tunable filter technologies with potential for high selectivity.

Figure 6.1(f) shows quasi-static tuning of the filter. By changing the control voltage into the phase shifter by only 0.75 V, the filter passband is shifted 3 GHz. The varying gain is attributed to the periodic optical filter used for carrier suppression in the SSB-SC block that also attenuates RF sideband signals that are close to the carrier. Important points are (a) the passband shape, bandwidth, and stopband attenuation (~30 dB) are similar to the filter response of Fig. 6.1(d), and (b) these quantities remain largely

unchanged when the filter is tuned. In accord with the predictions of eq. (6.1), the filter frequency may be tuned independently of the passband shape; this greatly simplifies high-speed tuning of such filters. This property has been demonstrated previously using a microwave delay-line filter with complex coefficients [81,82], but implementation complexity limited these filters to 2 taps, and fast tuning was not reported.

The novel blend of electronic technologies and optics in our setup enables tuning simultaneously at high speed and over broad bandwidth. To view the response of such rapidly time varying filters, a time domain measurement technique (as opposed to pervasive frequency domain methods based on network analyzers) is absolutely required.

Here we present two fast filtering demonstrations.

In the first demonstration, an RF test waveform in which a 3.7 GHz tone and a 1.8 GHz carrier subject to a 600 Mb/s binary phase shift keying modulation are superimposed and input into the SSB-SC modulator, and a high speed control signal is connected to the control port of the phase shifter. Figure 6.2(a) shows a high level view of the RF signal at the output of the photodiode and of the control signal to the RF phase shifter (shifted to account for the filter latency). The control signal comprises three different voltage levels that tune the filter to three different center frequencies. Zoomed-in sections of oscilloscope traces of the filter output, corresponding to high and mid level control voltages for which 3.7 and 1.8 GHz input signals are individually selected, are shown in Figs. 6.2(b) and 6.2(c), respectively. The low control voltage tunes the filter to a frequency band not present on the input signal, and the filter output goes low. Figure 6.2(d) shows a spectrogram of the data set, which provides an intuitive visual representation of the time-frequency character of the filtered signal. The spectrogram of the oscilloscope data was computed using a sliding FFT window of 20.4 ns duration, with contour lines drawn at 5-dB intervals down to 20 dB.

The different frequency components superimposed at the input are now separated in time, and the presence of modulation on the 1.8 GHz signal is clearly evident as an increased bandwidth. Examination of the rapid transitions between output frequency components reveals that the filter is able to switch within 40 ns, limited by the response time of the RF phase shifter. Such rapid filter tuning is unprecedented in RF photonics

and is substantially beyond the demonstrated capabilities of any known high selectivity filter technology.

In the second demonstration, an RF test waveform in which a 2.5 GHz tone and a 4 GHz tone are superimposed and input into the SSSB-SC modulator and a high speed control signal is connected to the control part of phase shifter. Similarly to (1), Fig. 6.3(a) shows the oscilloscope signal. Fig. 6.3(b) is the close up of the 2.5 GHz signal part and Fig. 6.3(c) is the close up of the 4 GHz signal part. Fig. 6.3(d) shows the spectrogram which indicates the filter switching speed is 40 ns.

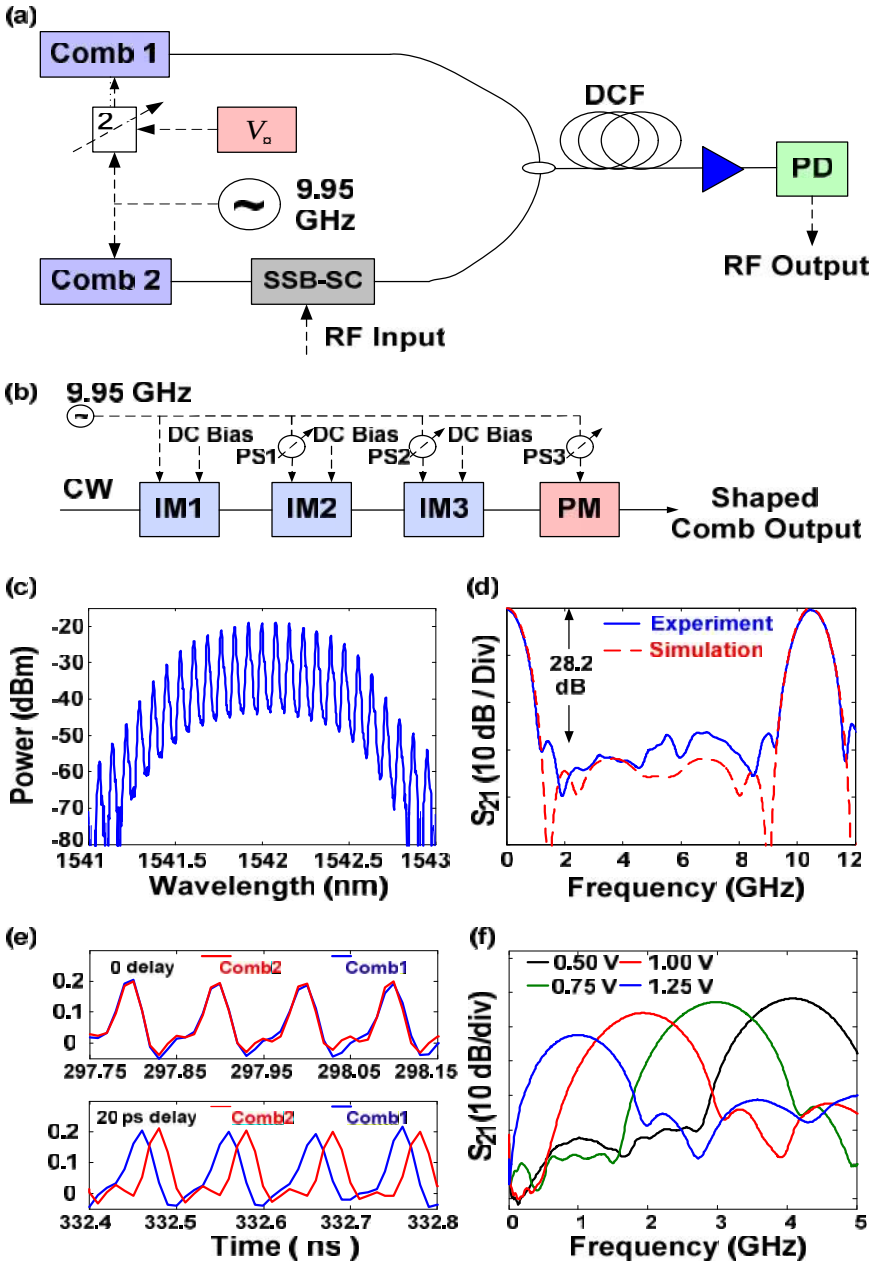

Fig. 6.1. Achieving rapid electronic frequency tunability of the RF filter using a dual-comb approach. a, Method to achieve rapid tunability using a dual comb scheme, b, Experimental scheme to directly generate a quasi-Gaussian shaped optical frequency comb. c, Experimentally measured optical spectrum of the frequency comb generated from b, and d, Measured (blue) and simulated (red) RF filter response using this comb. The vertical dashed lines depict individual Nyquist zones, where p is the zone number, explained under Methods. e, Experimental results showing the programmable rapid delay tuning between the two combs by applying a rapid step to the RF phase shifter, f, Tuning the center frequency of the RF filter by changing the voltage to the phase shifter (quasi-static case)

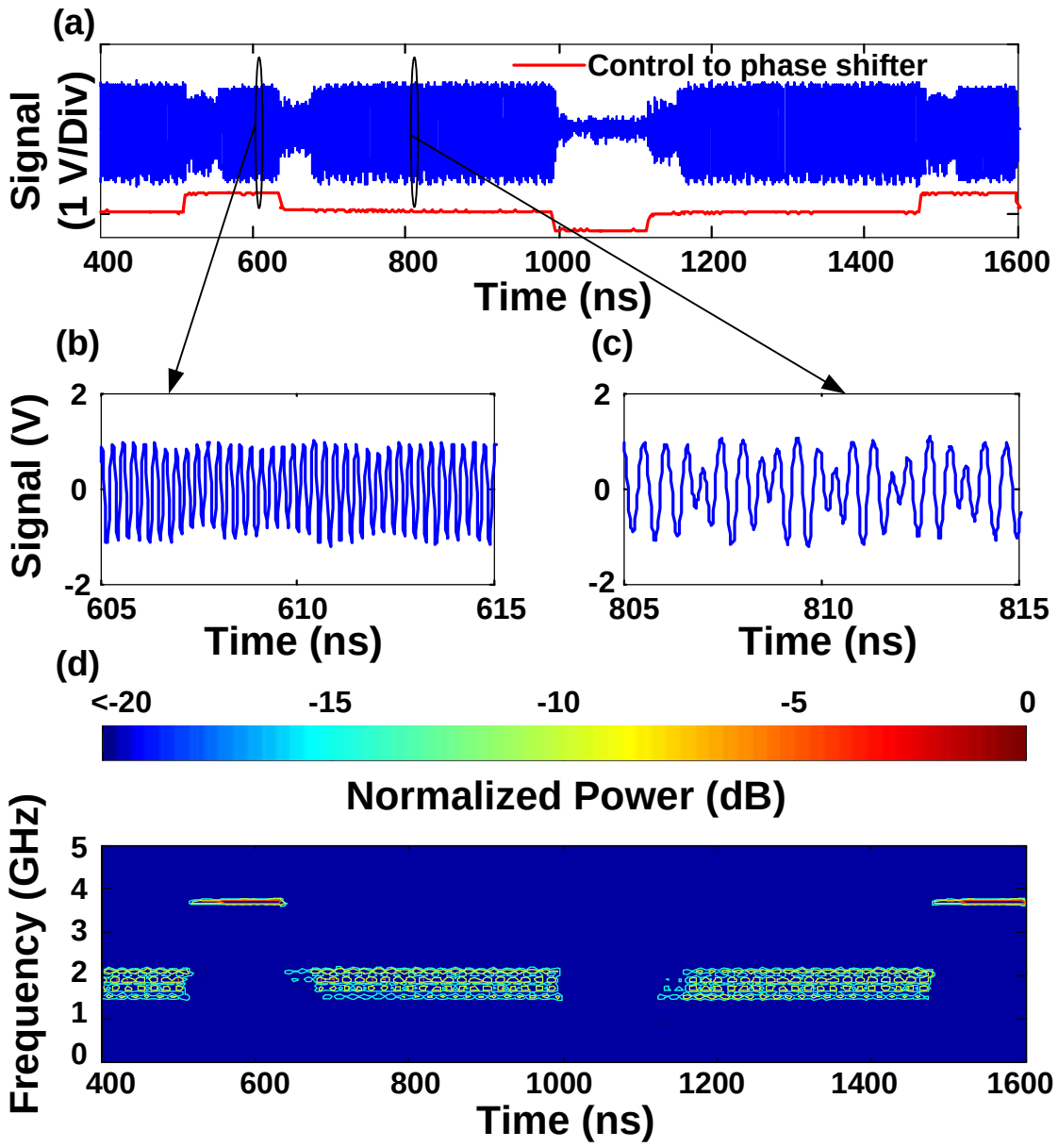

Fig. 6.2. Rapid frequency tunability of the RF filter. a, Measured oscilloscope signal demonstrating rapid switching between different frequency bands. Also shown is the control signal input to the phase shifter. b, Close up of a first waveform part of the signal - a 3.7 GHz RF tone c, Close up of a second waveform section – a 1.8 GHz RF tone undergoing binary phase shift keying at 600 Mb/s. d, Spectrogram representation of the filtered signal, highlighting rapid switching between different frequency bands.

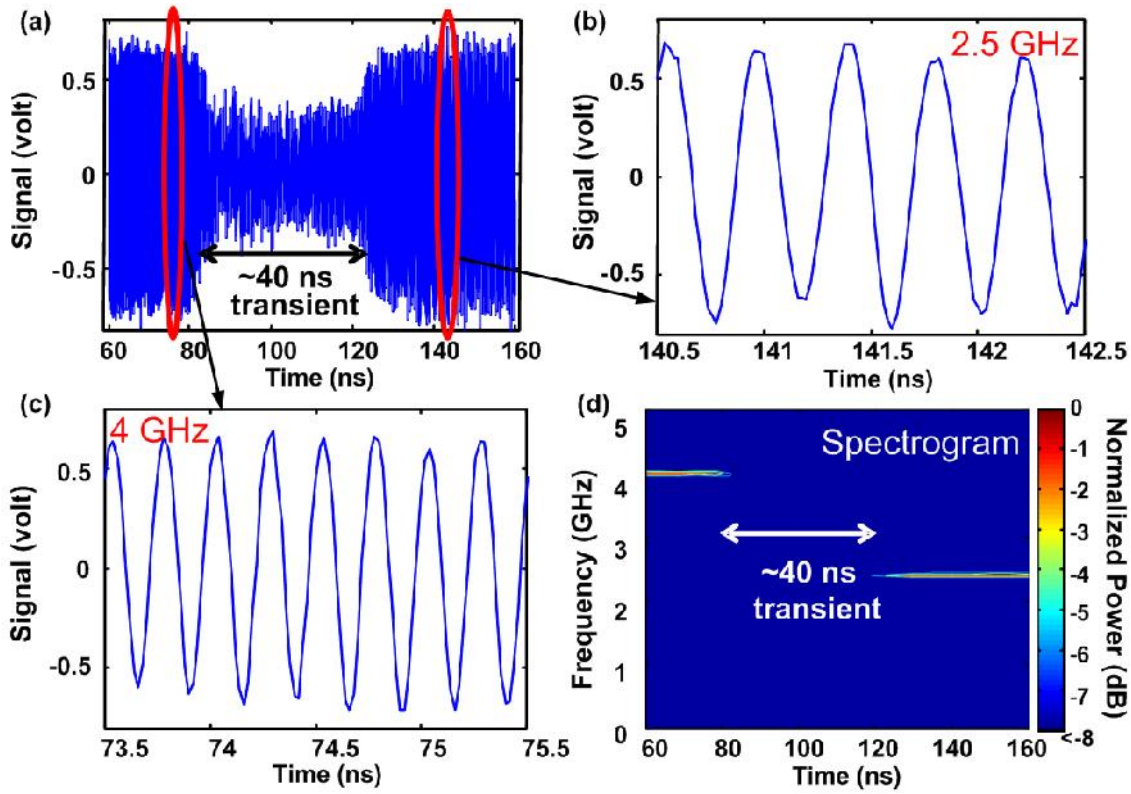

Fig. 6.3. Rapid frequency tunability of the RF filter (two-tone switching). a, Measured oscilloscope signal demonstrating rapid switching between different frequency bands. Also shown is the control signal input to the phase shifter. b, Close up of a first waveform part of the signal - a 2.5 GHz RF tone c, Close up of a second waveform section – a 4 GHz RF tone. d, Spectrogram representation of the filtered signal, highlighting rapid switching between different frequency bands.

7. SUMMARY AND DISCUSSION

In summary, we have demonstrated high quality 10 GHz flat-topped and Gaussian optical frequency combs with a series of intensity and phase modulators. Launching the Gaussian pulse from Gaussian-shaped comb into a length of HNLF with normal dispersion in the optical wave-breaking regime, we generate flat-topped optical frequency comb with ultrabroad bandwidth (>3.64 THz or 365 lines within 3.5 dB power variation), which covers the whole C-band. Exploiting the flexible electro-optically generated optical frequency combs, we have demonstrated several new principles for RF photonic filters. A novel nonlinear optics approach enhances both the bandwidth and shape of combs, leading to >60 dB MSSR and >70 dB RF stopband attenuation in a fixed filter geometry. Switching of optical delay under electronic control leads to extremely rapid (~40 ns) tuning of the filter response. We have also demonstrated 20 ns bandwidth reconfiguration of the RF photonic filter.

Some possible future improvements to extend the work in this dissertation are listed as follows:

1. Employing 10 GHz optical frequency comb limits the frequency span of our RF photonic filter that is free from Nyquist spurs to 5 Ghz, half of our 10-GHz comb repetition frequency [14]. We expect to increase the spur-free range of our RF photonic filters by employing higher frequency optical modulators.
2. Our filters exhibit approximately 40 dB RF insertion loss at 0.5 mA photodetector current, which is not good enough for practical applications [41]. However, increasing the photodetector current can decrease the RF insertion loss accordingly. Some possible solutions are using special low V_π modulators, high current handling detectors and low noise optical amplifier.

3. Although we have demonstrated new principles of RF photonic filters, the huge size of the filters prevents it from being in the commercial stage. However, photonic integration circuit (PIC) technology is mature, enabling integrating intensity modulators, phase modulators, optical amplifier, and many other components in our comb-based filter setup on a single chip possible in order to shrink the size.
4. We have demonstrated 20 ns RF bandwidth reconfiguration of our filter. The key enabling point is employing an electronically programmable RF variable attenuator with rapid switching speed. Using an alternative RF variable attenuator with faster switching speed will help achieve RF photonic filtering with <20 ns RF bandwidth reconfiguration.
5. We have demonstrate 40 ns RF passband frequency tuning of our filter. Similar to 4, using an alternative phase shifter with faster switching speed will help achieve RF photonic filtering with <40 ns passband frequency tuning speed.
6. We have achieved microwave photonic filtering with > 61 dB MSSR. Further enhancing the MSSR, for example >100 dB MSSR is very challenging. Simulation indicates three strategies are helpful to enhance the MSSR.
    - Increase the number of taps, equivalent to apply more phase modulation.
    - Narrow the pulse in time domain, equivalent to apply more intensity modulation.
    - Improve the phase profile for time to frequency mapping, equivalent to apply quasi-quadratic phase instead of sinusoidal phase.

Based on these three strategies, we starts with the scheme in section 5.2 and try to figure out schemes for higher MSSR with some minor modifications. For convenience, we use IMa to represent the intensity modulator biased at half Vπ driven with half Vπ RF amplitude. We use IMb to represent the intensity modulator biased at maximum transmission driven with Vπ RF amplitude.

(1) 1 IMa + 1 IMb + 1PM

Figure 7.1. shows the simulation results based on the scheme shown in Figure 5.2(a). Details about this scheme has been discussed in section 5.2. Figure 7.1.(a) shows the

comb spectrum driven by sinusoidal phase, the same as in chapter 5. Figure 7.1(b) shows the comb spectrum with the phase we correct to quasi-quadratic profile for a good time-to-frequency mapping. The comb spectrum is very obviously narrowed. Fig. 7.1(c) shows the RF filtering transfer function with comb 7.1(a) and comb 7.1(b) respectively. With comb 7.1(a), the expected filter response has a MSSR of 75 dB, 14 dB larger than our experimental result plotted in Fig. 4.3(c), due to the practically imperfect control of DC bias on IMs and power handling on both IMs and PMs. However based on simulation, we expect after improving the phase profile from sinusoidal to quasi-quadratic for comb 7.1(b), the MSSR of filtering response is improved by 10 dB.

(2) 2 IMa+1 IMb+ 1PM

Now based on the original scheme (1), let us add one IMa to narrow the pulse in time domain and see how the filter works. Figure 7.2(a) shows the comb spectrum driven by sinusoidal phase. Figure 7.2(b) shows the comb spectrum with quasi-quadratic phase profile. The combs do not look much different from those in Fig. 7.1. Fig. 7.2(c) shows the RF filtering transfer function with comb 7.2(a) and comb 7.2(b) respectively. With comb 7.2(a), the filter response has a MSSR of 115 dB, 40 dB larger than the one with single IMa. After improving the phase profile from sinusoidal to quasi-quadratic for comb 7.2(b), the MSSR of filtering response is increased to 130 dB!

(3) 2 IMa+1 IMb+ 2 PM

Now let us add one more phase modulator based on scheme (2). Fig. 7.3 (a) shows the comb spectrum driven by sinusoidal phase. Figure 7.3 (b) shows the comb spectrum with quasi-quadratic phase profile. With either sinusoidal phase or quasi-quadratic phase, the number of taps is significantly increased. Fig. 7.1.3 (c) shows the RF filtering transfer function with comb 7.3(a) and comb 7.3(b) respectively. With comb 7.3(a), the filter response has a MSSR of 122 dB. After improving the phase profile from sinusoidal to quasi-quadratic for comb 7.3(b), the MSSR of filtering response is increased to 145 dB! This scheme is very promising. The system setup is shown in Fig. 7.4 (a).

A key note here is we should be careful of the ratio between the first and second harmonics signals for quasi-quadratic phase generation. In chapter 2, the power of

second harmonic signal is 24 dB lower than the power of first harmonic signal for generating quasi-quadratic phase. However, since nonlinear process is involved in this scheme, for applying quasi-quadratic phase on the second cascaded FWM term, the power difference in the comb generator is not 24 dB any more.

We set the phase shifter in the red dashed module in Fig. 7.4(a) so that the phases to both combs from f_1 (: α_1) and f_2 (: α_2) before the single-mode fibers are proportional to:

$$\alpha_1 = \alpha_2 = \cos(2\mu t) - \sim \cos(\mu t) \tag{7.1}$$

Since we choose the length of SMF so that one pulse is delayed half period with respect to the other. Then after the SMF, we can regard α_1 reminds the same, but

$$\alpha_2 = \cos(2\mu t) + \sim \cos(\mu t) \tag{7.2}$$

After the nonlinear process in the HNLF, we select the second cascaded FWM comb term whose phase is proportional to

$$\alpha = 3\alpha_1 - 2\alpha_2 = \cos(2\mu t) - 5\sim \cos(\mu t) \tag{7.3}$$

which is quasi-quadratic phase. (7.3)

So α = 3.2. Then the power difference is $20*\log_{10}(3.2)$= 10.1 dB. This means for maximum modulation index, we put the power of first harmonic signal on each phase modulator to 30 dBm. The power of second harmonics signal on each phase modulator should be about 20 dBm. Then the results in Fig. 7.3. would be expected.

Now we investigate how if we change the power ratio between the first and second harmonic signals. After a large amount of simulations, we find that we can get larger MSSR through optimizing the ratio between the first and second harmonic signals to 0.8, which means the power difference is -1.9 dB as shown in Figure 7.4(b-d). Figure 7.4 (b) shows the comb spectrum with quasi-quadratic phase profile (α=3.2). Figure 7.4 (c) shows the comb spectrum with α=0.8. The number of taps is decreased. Fig. 7.4 (d) shows the RF filtering transfer function with comb 7.4(b) and comb 7.4(c) respectively. With comb 7.4(b), the filter response has a MSSR of 145 dB. With comb 7.5(c), the MSSR of filtering response is increased to 245 dB! This change is significant.

However we should notice largest modulation index should be applied to phase modulators for optimal result. In this case, if we put 30 dBm of first harmonic signal on

one phase modulator, we should put about 32 dBm of second harmonic signal on the phase modulator signal. Practically with our components, it is very difficult to put 32 dBm power of second harmonic signal on both phase modulators. So we propose to use one phase modulator instead of two phase modulators in the setup in Figure 7.5.

Figure 7.5 (a) shows a proposed setup. Figure 7.5 (b) and (c) show the comb spectrum with α=3.2, and α=0.8, respectively. Fig. 7.5 (d) shows the RF filtering transfer function with comb 7.5(b) and comb 7.5(c) respectively. With comb 7.5(b), the filter response has a MSSR of 130 dB. With comb 7.5(c), the MSSR of filtering response is increased to 200 dB.

Implementing these ideas is challenging experimentally. Low loss electro-optic intensity and phase modulators should be used in order to make sure the optical power at the Er-Yb doped high power amplifier before HNLF to >1mw level in order to make the signal amplified. Specially designed dispersion flattened highly nonlinear fiber should help for optimum performance [83].

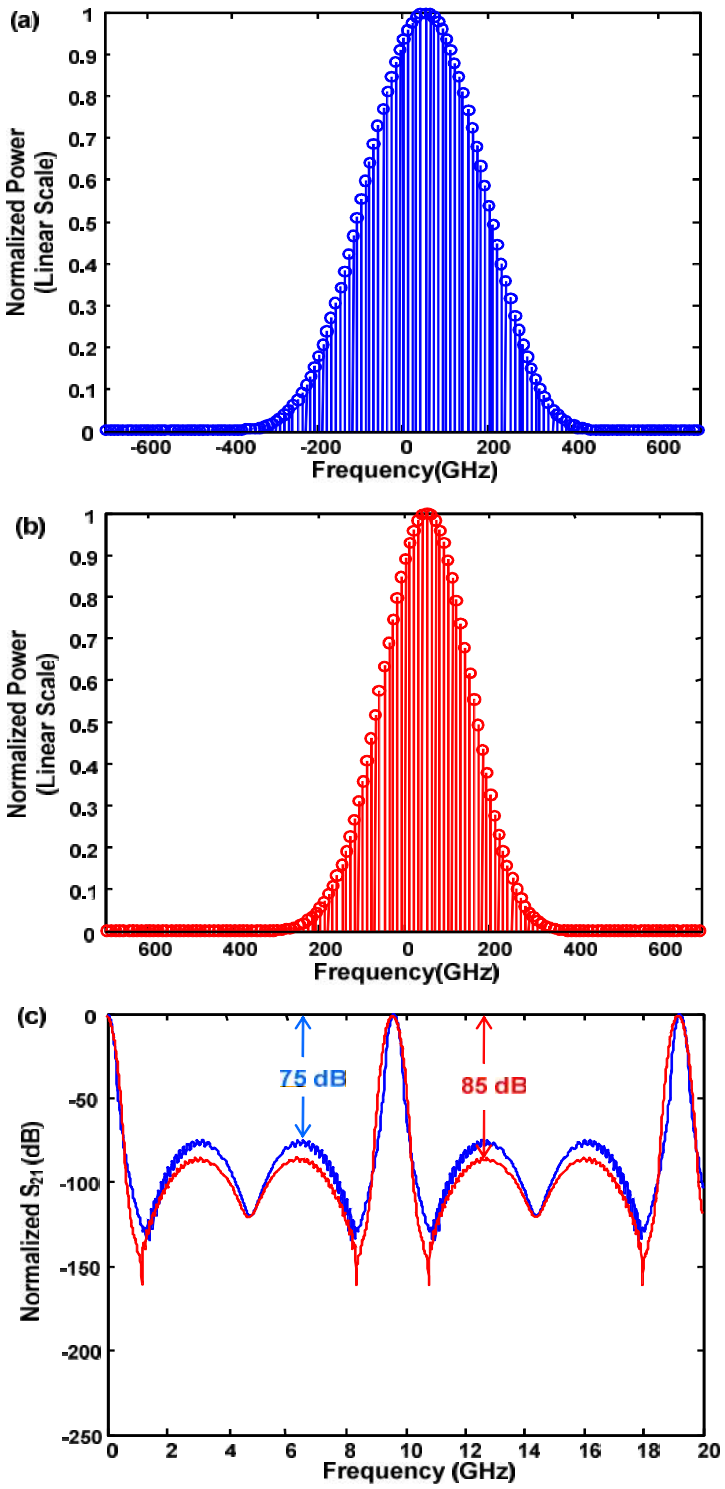

Fig. 7.1. Simulation results of RF photonic filtering with 1 IMa + 1 IMb + 1 PM (scheme in chapter 4). (a) Comb spectrum driven by sinusoidal phase, (b) Comb spectrum driven by quasi-quadratic phase, (c) RF filter transfer function. Blue: with comb (a), red: with comb (b).

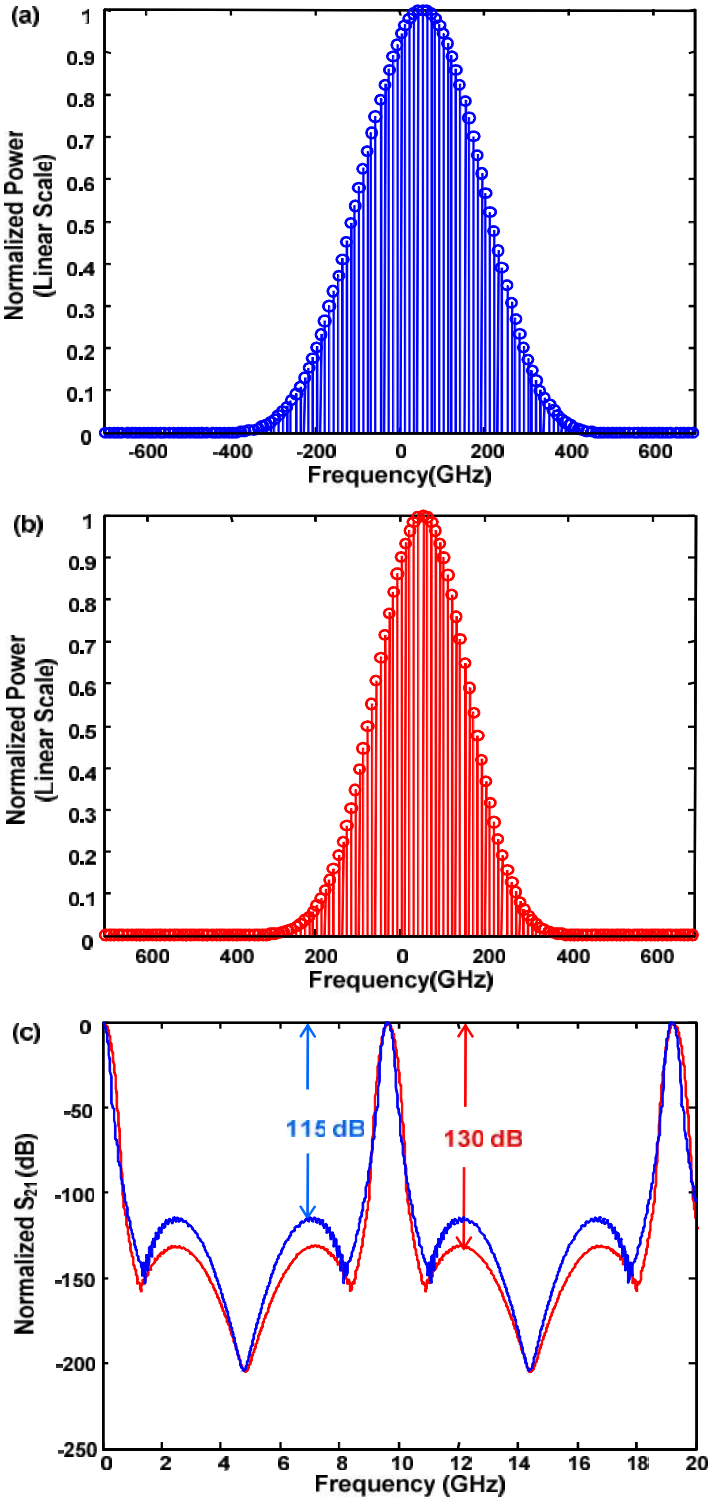

Fig. 7.2. Simulation results of RF photonic filtering with 2 IMa + 1 IMb + 1 PM. (a) Comb spectrum driven by sinusoidal phase, (b) Comb spectrum driven by quasi-quadratic phase, (c) RF filter transfer function. Blue: with comb (a), red: with comb (b).

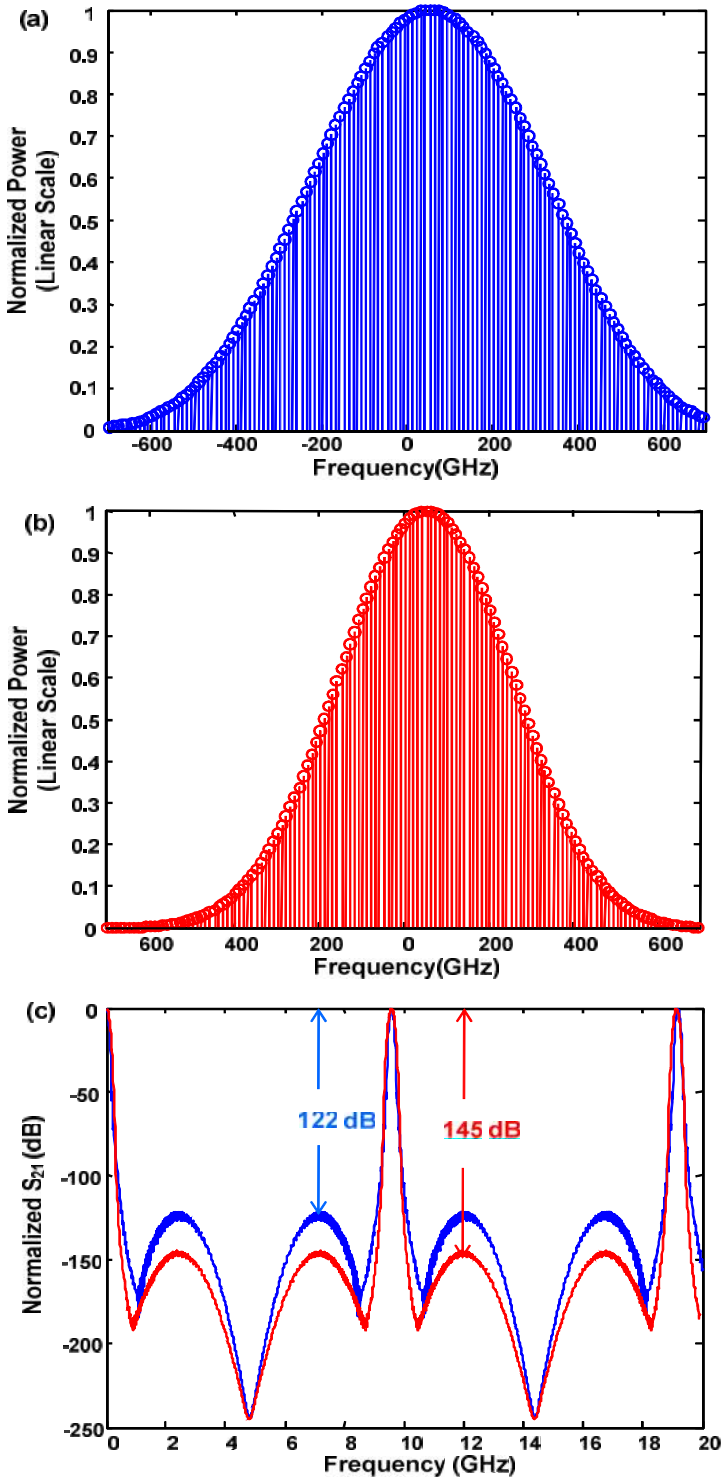

Fig. 7.3. Simulation results of RF photonic filtering with 2 IMa + 1 IMb + 2 PM. (a) Comb spectrum driven by sinusoidal phase, (b) Comb spectrum driven by quasi-quadratic phase, (c) RF filter transfer function. Blue: with comb (a), red: with comb (b).

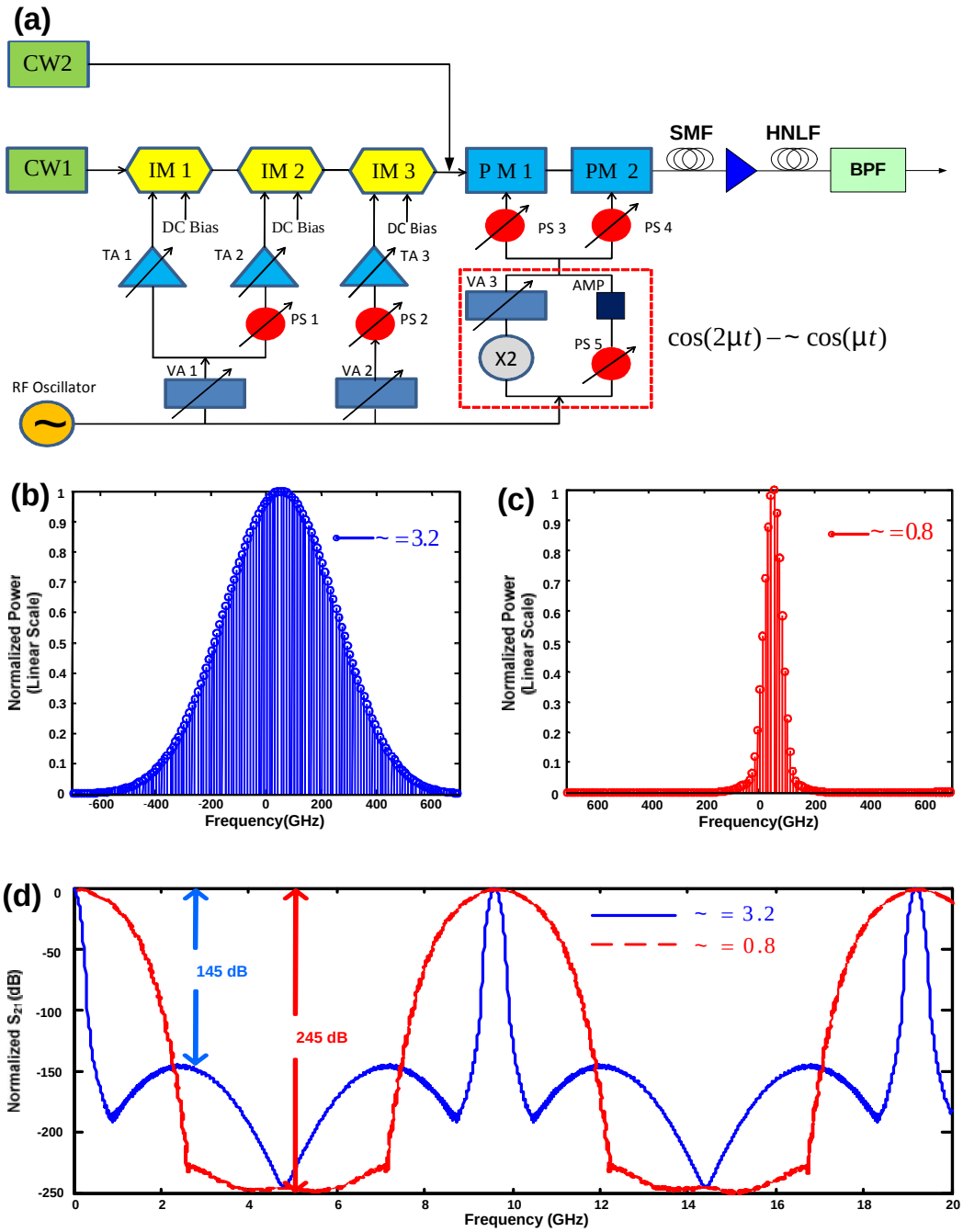

Fig. 7.4. Simulation results of RF photonic filtering with proposed experiment scheme: 2 IMa + 1 IMb + 2 PM with different power ratio between the first and second harmonics. (a), experiment setup, (b) Comb spectrum with α=3.2, (c) Comb spectrum with α=0.8, (d) RF filter transfer function. Blue: with comb (b), red: with comb (c).

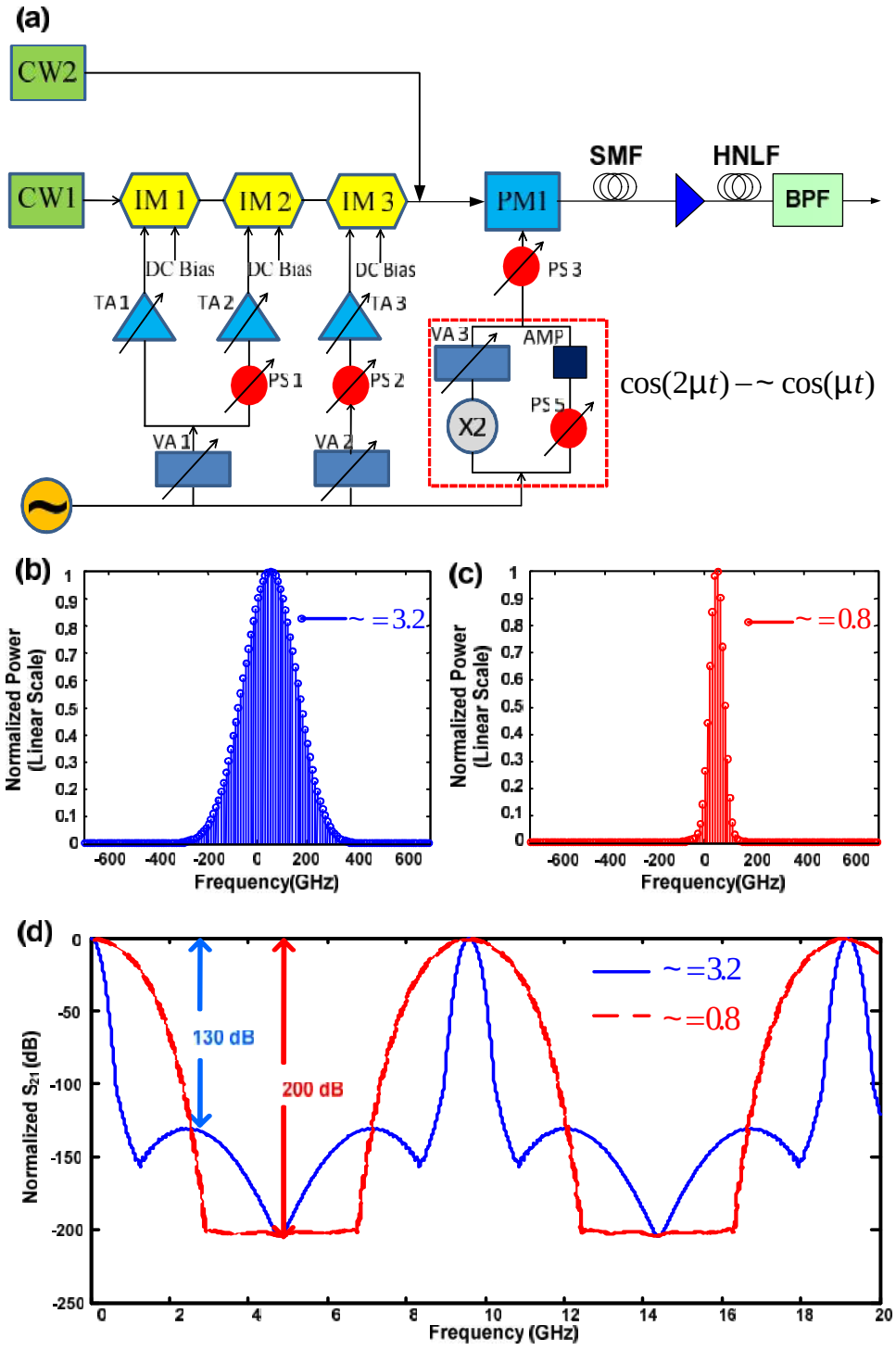

Fig. 7.5. Simulation results of RF photonic filtering with proposed experiment scheme: 2 IMa + 1 IMb + 1 PM with different power ratio between the first and second harmonics. (a), experiment setup, (b) Comb spectrum with α=3.2, (c) Comb spectrum with α=0.8, (d) RF filter transfer function. Blue: with comb (b), red: with comb (c).

LIST OF REFERENCES

LIST OF REFERENCES

[1] T. Udem, R. Holzwarth, and T. W. Hansch, “Optical frequency metrology,” Nature **416**, 233–237 (2002).

[2] D. J. Jones, S. A. Diddams, J. K. Ranka, A. Stentz, R. S. Windeler, J. L. Hall, and S. T. Cundiff, “Carrier-envelope phase control of femtosecond mode-locked lasers and direct optical frequency synthesis,” Science **288,** 635–639 (2000).

[3] L. S. Ma, Z. Bi, A. Bartels, L. Robertsson, M. Zucco, R. S. Windeler, G. Wilpers, C. Oates, L. Hollberg, and S. A. Diddams, “Optical frequency synthesis and comparison with uncertainty at the 10^{-19} level,” Science **303,** 1843–1845 (2004).

[4] J. Ye, and S. T. Cundiff, Femtosecond optical frequency comb: principle, operation, and applications (Springer, New York, 2005)

[5] N. R. Newbury, “Searching for applications with a fine-tooth comb,” Nature Photon. **5,** 186–188 (2011).

[6] P. J. Delfyett, S. Gee, M. Choi, H. Izadpanah, W. Lee, S. Ozharar, F. Quinlan, and T. Yilmaz, “Optical frequency combs from semiconductor lasers and applications in ultrawideband signal processing and communications,” J. Lightwave Technol. **24,** 2701–2719 (2006).

[7] A. D. Ellis, and F. C. G. Gunning, “Spectral density enhancement using coherent WDM,” IEEE Photon. Technol. Lett. **17(2),** 504–506 (2005).

[8] E. Yamazaki, F. Inuzuka, K. Yonenaga, A. Takada, and M. Koga, “Compensation of interchannel crosstalk induced by optical fiber nonlinearity in carrier phase-locked WDM system,” IEEE Photon. Technol. Lett. **19,** 9–11 (2007).

[9] Z. Jiang, C. Huang, D. E. Leaird, and A. M. Weiner, “Optical arbitrary waveform processing of more than 100 spectral comb lines, ” Nature Photon. **1,** 463–467 (2007).

[10] N. K. Fontaine, R. P. Scott, L. Zhou, F. M. Soares, J. P. Heritage, and S. J. B. Yoo, “Real-time full-field arbitrary optical waveform measurement,” Nature Photon. **4,** 248–254 (2010).

[11] S. T. Cundiff, and A. M. Weiner, “Optical Arbitrary Waveform Generation,” Nature Photon. **4,** 760–766 (2010).

[12] T. M. Fortier, M. S. Kirchner, F. Quinlan, J. Taylor, J. C. Bergquist, T. Rosenband, N. Lemke, A. Ludlow, Y. Jiang, C. W. Oates, and S. A. Diddams, “Generation of ultrastable microwave via optical frequency division,” Nature Photon. **5**, 425-429 (2011).

[13] C. B. Huang, D. E. Leaird, and A. M. Weiner, “Time-multiplexed photonically enabled radio-frequency arbitrary waveform generation with 100 ps transitions,” Opt. Lett. **32,** 3242–3244 (2007).

[14] E. Hamidi, D. E. Leaird, and A. M. Weiner, “Tunable programmable microwave photonic filters based on an optical frequency comb,” IEEE Trans. Microwave Theory Tech. **58,** 3269–3278 (2010).

[15] T. Ohara, H. Takara, T. Yamamoto, H. Masuda, T. Morioka, M. Abe, and H. Takahashi, “Over-1000-channel ultradense WDM transmission with supercontinuum multicarrier source,” J. Lightwave Technol. **24,** 2311–2317 (2006).

[16] R. Wu, V.R. Supradeepa, C. M. Long, D. E. Leaird, and A. M. Weiner, “Generation of very flat optical frequency combs from continuouswave lasers using cascaded intensity and phase modulators driven by tailored radio frequency waveforms,” Opt. Lett. **35,** 3234–3236 (2010)

[17] J. Capmany, B. Ortega, and D. Pastor, “A tutorial on microwave photonic filters,” J. Lightw. Technol. **24**, 201–229 (2006).

[18] G. M. Rebeiz, RF MEMS: Theory, Design, and Technology (John Wiley & Sons, New Jersey, 2003)

[19] S. J. Park, I. Reines, C. Patel, and G. M. Rebeiz, “High-Q RF-MEMS 4-6-GHz tunable evanescent-mode cavity filter,” IEEE Trans. Microwave Theory Tech. **58,** 381–389 (2010).

[20] X. Liu, L. P. B. Katehi, W. J. Chappell, and D. Peroulis, “High-Q tunable microwave cavity resonators and filters using SOI-based RF MEMS tuners,” IEEE J. Microelectromesh. Syst. **19,** 774–784 (2010).

[21] B. Kaa, “A simple approach to YIG oscillators,” VHF Communications, pp. 217-224 (2004)

[22] J. Nath, D. Ghosh, J. Maria, A. I. Kingon, W. Fathelbab, P. D. Franzon, and M. B. Steer, “An electronically tunable microstrip bandpass filter using thin-film barium-strontium-titanate (BST) varactors,” IEEE Trans. Microwave Theory Tech. **53,** 2707–2712 (2005).

[23] S. H. Talisa, M. A. Janocko, C. Moskowitz, J. Talvacchio, J. F. Billing, R. Brown, D. C. Buck, C. K. Jones, B. R. McAvoy, G. R. Wagner, and D. H. Watt, "Low- and high-temperature superconducting microwave filters," IEEE Trans. Microwave Theory Tech. **39,** 1448–1454 (1991).

[24] W. Yan, and R. R. Mansour, "Tunable dielectric resonator bandpass filter with embedded MEMS tuning elements," IEEE Trans. Microwave Theory Tech. **55,** 154–160 (2007).

[25] A. Wong, H. Ding, and C. Nguyen, "Micromechanical mixer and filters," Technical digest of Electron devices meeting, pp. 471-474. (1998)

[26] A. J. Seeds, and K. J. Williams, "Microwave photonics," J. Lightwave Technol. **24,** 4628–4641 (2006).

[27] J. Capmany, and D. Novak, "Microwave photonics combines two worlds," Nature Photon. **1,** 319–330 (2007).

[28] J. P. Yao, "Microwave photonics," J. Lightwave Technol. **27,** 314–335 (2009).

[29] S. Haykin, "Cognitive radio: brain-empowered wireless communications," IEEE J. Select. Areas Commun. **23,** 201–220 (2005).

[30] I. F. Akyildiz, W. Y. Lee, M. C. Vuran, and S. Mohanty, "NeXt generation/dynamic spectrum access/cognitive radio wireless networks: A survey," Comput. Networks **50,** 2127–2159 (2006).

[31] R. A. Minasian, "Photonic signal processing of microwave signals," IEEE Trans. Microwave Theory Tech. **54,** 832–846 (2006).

[32] J. Capmany, B. Ortega, D. Pastor, and S. Sales, "Discrete-time optical processing of microwave signals," J. Lightwave Technol. **23,** 702–723 (2005).

[33] C. K. Madsen, and J. H. Zhao, Optical filter design and analysis: a signal processing approach (Wiley, New York, 1999).

[34] F. J. Harris, "On the use of windows for harmonic analysis with the discrete fourier transform," Proc. IEEE **66,** 51–83 (1978).

[35] A. V. Oppenheim, and R. W. Schafer, Discrete-time signal processing 3rd edn (Prentice-Hall, New Jersey, 2009).

[36] A. Ortigosa-Blanch, J. Mora, J. Capmany, B. Ortega, and D. Pastor, "Tunable radio-frequency photonic filter based on an actively mode-locked fiber laser," Opt. Lett. **31,** 709–711 (2006).

[37] L. H. Lee, Y. M. Chang, Y. G. Han, S. B. Lee, and H. Y. Chung, "Fully reconfigurable photonic microwave transversal filter based on digital micromirror device and continuous-wave, incoherent supercontinuum source," Appl. Opt. **46,** 5158–5167 (2007).

[38] M. Song, V. Torres-Company, and A. M. Weiner, "Noise comparison of RF photonic filters based on coherent and incoherent multiwavelength sources," IEEE Photon. Tech. Lett. **24**, 1236-1238 (2012).

[39] A. M. Weiner, "Femtosecond pulse shaping using spatial light modulators," Rev. Sci. Instr. **71,** 1929–1960 (2000).

[40] G. H. Smith, D. Novak, and A. Zaheer, "Overcoming chromatic-dispersion effects in fiber-wireless systems incorporating external modulators," IEEE Trans. Microwave Theory Tech. **45,** 1410–1415 (1997).

[41] V.R. Supradeepa*, C. M. Long*, R. Wu*, F. Ferdous, E. Hamidi, D. E. Leaird, and A. M. Weiner, "Comb-based radiofrequency photonic filters with rapid tunability and high selectivity," Nature Photon. **6**, 186-194 (2012). [*These authors contributed equally to this work.]

[42] T. Yamamoto, T. Komukai, K. Suzuki, and T. Atsushi, "Multicarrier light source with flattened spectrum using phase modulators and dispersion medium," J. Lightwave Technol. **27**, 4297-4305 (2009).

[43] T. Sakamoto, T. Kawanishi, and M. Izutsu, "Widely wavelength-tunable ultra-flat frequency comb generation using conventional dual-drive Mach-Zehnder modulator," Electron. Lett. **43,** 1039-1040 (2007).

[44] S. Ozharar, F. Quinlan, I. Ozdur, S. Gee, and P. J. Delfyett, "Ultrafast optical comb generation by phase-only modulation of continuous-wave light," IEEE Photon. Technol. Lett. **20**, 36-38 (2008).

[45] S. Hisatake, K. Tada, and T. Nagatsuma, "Generation of an optical frequency comb with a Gaussian spectrum using a linear time-to-space mapping system," Opt. Express **18,** 4748-4757 (2010)

[46] R. Wu, C. M. Long, D. E. Leaird, and A. M. Weiner, "Directly generated Gaussian-shaped optical frequency comb for microwave photonic filtering and picoseconds pulse generation," IEEE Photon. Technol. Lett. **24**, 1484-1486 (2012)

[47] R. Wu, V. Torres-Company, D. E. Leaird, and A. M. Weiner, "Supercontinuum-based 10-GHz flat-topped optical frequency comb generation," Opt. Express **21**, 6045-6052 (2013).

[48] J. Azaña, N. K. Berger, B. Levit, and B. Fischer, "Spectro-temporal imaging of optical pulses with a single time lens," IEEE Photon. Technol. Lett. **16,** 882-884 (2004).

[49] V. Torres-Company, J. Lancis, and P. Andrés, "Lossless equalization of frequency combs," Opt. Lett. **33,** 1822–1824 (2008).

[50] J. V. Howe, J. Hansryd, and C. Xu, "Multiwavelength pulse generator using time-lens compression," Opt. Lett. **29**, 1470–1472 (2004).

[51] V.R. Supradeepa, C. M. Long, D. E. Leaird, and A. M. Weiner, "Self-referenced characterization of optical frequency combs and arbitrary waveforms using a simple, linear, zero-delay implementation of spectral shearing interferometry," Opt. Express **18,** 18171-18179 (2010).

[52] K. Tamura, H. Kubota, and M. Nakazawa, "Fundamentals of stable continuum generation at high repetition rates," J. Lightwave Technol. **36**(7), 773-779 (2000).

[53] Y. Takushima, and K. Kikuchi, "10-GHz, over 20-channel multiwavelength pulse source by slicing super-continuum spectrum generated in normal-dispersion fiber," IEEE Photon. Technol. Lett. **11**(3), 322-324 (1999).

[54] F. Parmigiani, C. Finot, K. Mukasa, M. Ibsen, M. Roelens, P. Petropoulos, and D. J. Richardson, "Ultra-flat SPM-broadened spectra in a highly nonlinear fiber using parabolic pulses formed in a fiber Bragg grating," Opt. Express **14**(17), 7617-7622 (2006).

[55] A. Clarke, D. Williams, M. Roelens, and B. Eggleton, "Reconfigurable optical pulse generator employing a fourier-domain programmable optical processor," IEEE Photon. Technol. Lett. **28**(1), 97-103 (2010).

[56] X. Yang, D. J. Richardson, and P. Petropoulos, "Nonlinear generation of ultra-flat broadened spectrum based on adaptive pulse shaping," J. Lightwave Technol. **30**(12), 1971-1977 (2012).

[57] K. Kashiwagi, H. Ishizu, Y. Kodama, S. Choi, and T. Kurokawa, "Highly precise optical pulse synthesis for flat spectrum supercontinuum generation with wide mode spacing," in European Conference on Optical Communication (ECOC), We.7.E.5 (2010).

[58] H. Tsuda, Y. Tanaka, T. Shioda, and T. Kurokawa, "Analog and digital optical pulse synthesizers using arrayed-waveguide gratings for high-speed optical signal processing," J. Lightwave Technol. **26**(6), 670-677 (2008).

[59] Y. Tanaka, R. Kobe, T. Kurokawa, T. Shioda, and H. Tsuda, "Generation of 100-Gb/s packets having 8-bit return-to-zero patterns using an optical pulse synthesizer with a lookup table," IEEE Photon. Technol. Lett. **21**(1), 39-41 (2009).

[60] V.R. Supradeepa, and A. M. Weiner, “Bandwidth scaling and spectral flatness enhancement of optical frequency combs from phase-modulated continuous-wave lasers using cascaded four-wave mixing,” Opt. Lett. **37**(15), 3066-3068 (2012).

[61] M. Song, V. Torres-Company, A. J. Metcalf, and A. M. Weiner, “Multitap microwave photonic filters with programmable phase response via optical frequency comb shaping,” Opt. Lett. **37**(5), 845-847 (2012).

[62] M. Song, R. Wu, V. Torres-Company, D. E. Leaird, and A. M. Weiner, “Programmable microwave photonic phase filters with large time-bandwidth product based on ultra-broadband optical frequency comb generation,” in Microwave Photonics (MWP), 2012 IEEE Topical Meeting (2012).

[63] G. P. Agrawal, Nonlinear Fiber Optics, 4th ed. (Academic, 2007).

[64] C. Finot, B. Kibler, L. Provost, and S. Wabnitz, “Beneficial impact of wave-breaking for coherent continuum formation in normally dispersive nonlinear fibers,” J. Opt. Soc. Am. B **25**(11), 1938-1948 (2008).

[65] W. Tomlinson, R. Stolen, and A. Johnson, “Optical wave breaking of pulses in nonlinear optical fibers,” Opt. Lett. **10**(9), 457-459 (1985).

[66] Y. Liu, H. Tu, and S. Boppart, “Wave-breaking-extended fiber supercontinuum generation for high compression ratio transform-limited pulse compression,” Opt. Lett. **37**(12), 2172-2174 (2012).

[67] C. B. Huang, S. G. Park, D. E. Leaird, and A. M. Weiner, “Nonlinear broadened phase-modulated continuous-wave laser frequency combs characterized using DPSK decoding,” Opt. Express **16**(4), 2520-2527 (2008).

[68] J. P. Heritage, R. N. Thurston, W. J. Tomlinson, A. M. Weiner, and R. H. Stolen, “Spectral windowing of frequency-modulated optical pulses in a grating compressor,” Appl. Phys. Lett. **47**(2), 87-89 (1985).

[69] A. M. Weiner, Ultrafast Optics (Wiley, 2009), Chap. 3.

[70] H. Joshi, H. H. Sigmarsson, S. Moon, D. Peroulis, and W. J. Chappell, "High Q Narrowband Tunable Filters With Controllable Bandwidth," IEEE MTT-S International Microwave Symposium Digest, 629-632 (2009)

[71] M. Sánchez-Renedo, R. Gómez-Garc´ıa, J. I. Alonso, and C. Briso-Rodr´ıguez, “Tunable combline filter with continuous control of center frequency and bandwidth,” IEEE Trans.Microw. Theory Tech. 53, 191–199 (2005)

[72] C. H. Kim, and K. Chang, “Ring resonator bandpass filter with switchable bandwidth using stepped-impedance stubs,” IEEE Trans. Microw. Theory Tech. 58, 3936–3944 (2010)

[73] C. Rauscher, "Reconfigurable bandpass filter with a three-toone switchable passband width," IEEE Trans. Microw. Theory Tech. 51, 573-577 (2003)

[74] X. Huang, Q. Feng, and Q. Xiang, “Bandpass filter with tunable bandwidth using quadruple-mode stub-loaded resonator,” IEEE Trans. Microw. Wireless Compon. Lett. 22, 176–178 (2012)

[75] W. Tu, "Compact low-loss reconfigurable bandpass filter with switchable bandwidth," IEEE Trans. Microw. Wireless Compon. Lett. 20, 208-210 (2010)

[76] A. L. C. Serrano, F. S. Correra, T. Vuong, and P. Ferrari, “Synthesis methodology applied to a tunable patch filter with independent frequency and bandwidth control,” IEEE Trans. Microw. Theory Tech. 60, 484–493 (2012)

[77] C. Lugo and J. Papapolymerou, “Single switch reconfigurable bandpass filter with variable bandwidth using a dual-mode triangular patch resonator,” in Proc. IEEE MTT-S Int. Microw. Symp. Dig. 779–782 (2005)

[78] E.H.W. Chan, and R. A. Minasian, “Coherence-free high-resolution RF/microwave photonic bandpass filter with high skirt selectivity and high stopband attenuation,” J. Lightwave Tech. 28, 1646–1651 (2010).

[79] A. A. Savchenkov, W. Liang, V. Ilchenko, A. B. Matsko, D. Seidel, and L. Maleki, “RF photonic signal processing components: From high order tunable filters to high stability tunable oscillators,” Proc. of 2009 IEEE Radar Conference 1, 1–6 (2009).

[80] V. Ilchenko, and L. Maleki, Tunable radio frequency and microwave photonic filters. US-Patent 7,813,651 B2 (2010)

[81] A. Loayssa, J. Capmany, M. Sagues, and J. Mora, “Demonstration of incoherent microwave photonic filters with all-optical complex coefficients,” IEEE Photon. Technol. Lett. 18, 1744–1746 (2006).

[82] Y. Yan, and J. P. Yao, “A tunable photonic microwave filter with a complex coefficient using an optical RF phase shifter,” IEEE Photon. Technol. Lett. **19,** 1472–1474 (2007).

[83] V. Ataie, B. Kuo, E. Myslivets, and S. Radic, “Generation of 1500-tone, 120nm-wide ultraflat frequency comb by single CW source,” paper PDP5C.1, Proc. of 2013 OFC/NFOEC (2013)

VITA

VITA

Rui Wu received the B. E. degree in Electrical Engineering from Shanghai Jiaotong University (SJTU), Shanghai, China, in 2008. Rui is currently working toward the PhD degree under the direction of Prof. Andrew M. Weiner in the School of Electrical and Computer Engineering at Purdue University, West Lafayette, IN, USA. He has been a research assistant in the Ultrafast Optics and Optical Fiber Communication Laboratory since 2008. His current research interests include radio frequency photonics, ultrafast optics, optical frequency comb source development, silicon photonics, etc. He was an exchange student at University of California, Los Angeles (UCLA) in 2007 summer. He was a summer research intern at NEC Laboratories America in Princeton, NJ from May 2012 to August 2012.

During the course of his graduate study, Rui Wu has authored and co-authored more than 20 publications in peer reviewed journals and international conferences. In August 2012, he was invited to give a seminar about his research for the Columbia Optics and Quantum Electronics Seminar at Columbia University (New York, NY). He is a student member of IEEE and IEEE Photonics Society. He was nominated as a student paper finalist in 2010 IEEE International Topical Meeting on Microwave Photonics. He received travel grant award for 2010 IEEE Photonics Society Annual Meeting. His paper was one of the ten top downloads in Optics Express in March 2013. He has served as a reviewer for more than 30 times for IEEE Photonics Technology Letters, Optics Letters, Optics Express, Journal of Lightwave Technology, Optics Communications, IEEE Microwave and Wireless Components Letters, IEEE Sensor Journal, and Chinese Optics Letters.